Available online at www.sciencedirect.com

SciVerse ScienceDirect

Geochimica et Cosmochimica Acta 97 (2012) 88–104

Geochimica et Cosmochimica Acta

www.elsevier.com/locate/gca

Silicon isotope constraints on sources and utilization of silicic acid in the northern South China Sea

Zhimian Cao [a], Martin Frank [b], Minhan Dai [a,*], Patricia Grasse [b], Claudia Ehlert [b]

[a] State Key Laboratory of Marine Environmental Science, Xiamen University, Daxue Road 182, Xiamen 361005, China
[b] GEOMAR|Helmholtz Center for Ocean Research Kiel, Wischhofstrasse 1-3, Kiel 24148, Germany

Received 14 November 2011; accepted in revised form 29 August 2012; Available online 9 September 2012

Abstract

The stable silicon isotopic composition ($\delta^{30}Si$) of waters and diatoms has increasingly been used to investigate the biogeochemical cycling of Si in the major ocean basins. Here we present the first Si isotope data set from the northern South China Sea (NSCS), a large marginal sea system in the western North Pacific to examine sources and utilization of silicic acid ($Si(OH)_4$). During two cruises in July–August 2009 (summer) and January 2010 (winter), samples for isotope measurements of dissolved $Si(OH)_4$ ($\delta^{30}Si_{Si(OH)_4}$) and of biogenic silica ($\delta^{30}Si_{BSi}$) in suspended particles were collected along a transect perpendicular to the coast from the inner shelf to the deep-water slope, as well as at the South East Asian Time-series Study (SEATS) station located in the NSCS basin. Surface $\delta^{30}Si_{Si(OH)_4}$ generally increased from values ~+2.3‰ on the inner shelf to ~+2.8‰ above the deep basin, suggesting an increasing utilization of dissolved $Si(OH)_4$ reflecting the transition from eutrophic to oligotrophic conditions. The $\delta^{30}Si_{BSi}$ values were systematically lower than the corresponding $\delta^{30}Si_{Si(OH)_4}$ in the euphotic zone (above 100 m) on the shelf and slope. In contrast at station SEATS in the NSCS basin, $\delta^{30}Si_{BSi}$ signatures in both seasons were within error equal to $\delta^{30}Si_{Si(OH)_4}$ in the surface mixed layer (above 50 m) and $\delta^{30}Si_{BSi}$ in waters below were significantly higher than the corresponding $\delta^{30}Si_{Si(OH)_4}$. By comparing the field data with the Si isotope fractionation revealed by the Rayleigh or the steady state models, we demonstrate the existence of variable $Si(OH)_4$ origins in different areas of the NSCS. Surface waters on the inner shelf were largely fed by nutrients from the Pearl River input. While the primary source of $Si(OH)_4$ for the euphotic zone on the outer shelf and slope was upwelling or vertical mixing from underlying waters, the $Si(OH)_4$ in the surface mixed layer of the NSCS basin might have originated from horizontal mixing with other highly fractionated surface waters. As a consequence, the Si isotope dynamics in the NSCS are largely controlled by variable biological fractionation of Si in waters from different sources with different initial Si isotopic compositions rather than any single source water.

1. INTRODUCTION

Diatoms contribute to over half of the primary production (PP) in high nutrient and coastal regions where they dominate the cycling of both silicon (Si) and carbon (C) (Nelson et al., 1995). However, our current understanding of the biogeochemical cycle of Si is limited relative to that of C and nitrogen (N), partly due to the technical difficulty of making direct measurements of particulate biogenic silica (BSi) production and dissolution rates in the ocean (Brzezinski and Phillips, 1997; Fripiat et al., 2009).

Examining natural variations of the stable Si isotopic composition ($\delta^{30}Si$) provides an alternative tool for studying the oceanic Si cycle. It is possible to resolve processes, such as silicic acid ($Si(OH)_4$) utilization, BSi dissolution and water mass mixing (e.g., Cardinal et al., 2005; Reynolds et al., 2006; Beucher et al., 2008, 2011; Fripiat et al., 2011b). Both field studies (Fripiat et al., 2011b, and references therein) and laboratory culture experiments (De La Rocha et al., 1997) have revealed that diatoms preferentially incor-

* Corresponding author. Tel.: +86 592 2182132; fax: +86 592 2184101.
E-mail address: mdai@xmu.edu.cn (M. Dai).

0016-7037/$ - see front matter © 2012 Elsevier Ltd. All rights reserved.
http://dx.doi.org/10.1016/j.gca.2012.08.039

porate lighter Si isotopes (i.e., ^{28}Si) from surrounding seawater with an essentially constant fractionation factor ($^{30}\varepsilon_{upt}$) of −1.1‰. Via culture experiments, Demarest et al. (2009) demonstrate that stable Si isotope fractionation also occurs during BSi dissolution whereby the lighter Si isotopes are preferentially released into seawater ($^{30}\varepsilon_{diss} = -0.55‰$). While nearly all field studies have so far been conducted in the open ocean, such as in the Southern Ocean (Varela et al., 2004; Cardinal et al., 2005, 2007; Cavagna et al., 2011; De La Rocha et al., 2011; Fripiat et al., 2011a, 2011b, 2012), the Pacific Ocean (Reynolds et al., 2006; Beucher et al., 2008, 2011) or the Atlantic Ocean (de Souza et al., 2012), extensive $\delta^{30}Si$ data, except for one profile from the Monterey Bay (De La Rocha et al., 2000), have not yet been obtained in coastal oceans where diatoms are ecologically and biogeochemically more important and dynamic.

The South China Sea (SCS) is the world's largest tropical–subtropical marginal sea covering an area of 3.5×10^6 km^2. Its semi-enclosed deep basin is permanently stratified with a very shallow mixed layer depth (typically <50 m). It is oligotrophic with extremely low levels of surface inorganic nutrients (nitrate and phosphate concentrations are at nM level) and thus dominated by picophytoplankton (<2 μm in size) contributing up to 50–75% of the total chlorophyll *a* concentration (Ning et al., 2004). In contrast, the wide shelves at the northwestern and southern boundaries receive large riverine inputs of nutrients leading to enhanced biological productivity (Han et al., 2012). For instance, the nutrient fluxes from the Pearl River to the inner shelf of the northern SCS (NSCS) significantly raise the surface nitrate concentrations to the μM level (Cai et al., 2004; Dai et al., 2008; Han et al., 2012). The resulting relatively eutrophic conditions are conducive to the growth of micro-phytoplankton (>20 μm in size), such as diatoms, which account for 48–63% of the total chlorophyll *a* concentration in the nearshore waters of the NSCS (Chen et al., 2006). As a consequence, the absolute abundance of diatoms generally decreases from the shelf to the deep basin of the NSCS (Chen et al., 2006), which reflects spatial variations of the diatom productivity. Moreover, it is estimated that on the NSCS shelf the diatom cell density in winter is slightly higher than in summer, whereas in the central basin the winter values are nearly five times higher than during summer (see Chen, 2005, Table 8), indicating a large seasonal variation of the diatom productivity in the SCS.

In the context of such complex hydrographic conditions, besides the changing roles that diatoms play in different areas and/or seasons, stable Si isotopes are potentially able to better resolve the various physical and biological processes controlling the Si cycle in the SCS. In this study, $\delta^{30}Si$ data for dissolved seawater $Si(OH)_4$ ($\delta^{30}Si_{Si(OH)_4}$) and BSi in suspended particles ($\delta^{30}Si_{BSi}$) were collected in July–August 2009 (summer) and January 2010 (winter) at the same stations in the NSCS, extending from the inner shelf into the deep basin. On the basis of these field data and samples, we for the first time systematically investigated $\delta^{30}Si$ signatures and their relevance to $Si(OH)_4$ sources and utilization in a coastal sea. These data are put into perspective with the variable spatial and seasonal differences of the physico-biogeochemical conditions.

2. MATERIALS AND METHODS

2.1. Study area

The East Asian Monsoon prevails in the SCS resulting in a seasonal reversal of surface circulation with a cyclonic gyre in winter and an anticyclonic gyre during summer (Fig. 1). As a consequence, the interior of the SCS is effectively isolated from terrestrial inputs and forms a basin-wide gyre, which displays overall oligotrophic characteristics similar to those in the major ocean basins (Gong et al., 1992). On the other hand, the SCS basin is connected with the western North Pacific (wNP) via the 2200 m deep Luzon Strait, through which the Kuroshio Branch Water intrudes from the wNP into the SCS (Dai et al., 2009, and references therein) (Fig. 1). Amongst various rivers in southern China feeding the NSCS shelf, the Pearl River (Fig. 1) is one of the world's largest major river systems with a water discharge of 3.26×10^{11} m^3 yr^{-1}. It is noted that ~80% of the discharge takes place during the wet season (April–September) (Guo et al., 2008; Cao et al., 2011).

2.2. Sampling and analysis

2.2.1. Cruise and sampling

Sampling was conducted onboard the R/V *Dongfanghong* II during both the summer (from July 19 to August 16, 2009) and winter (January 6 to 30, 2010) cruises to the NSCS organized by the CHOICE-C project (Carbon cycling in China Seas – budget, controls and ocean acidification). In both cruises, samples for Si isotopes were collected at the South East Asian Time-series Study (SEATS) station established in the NSCS basin, and at stations A9, A7, A5, A2, and A10 along transect A extending from the shore near the mouth of the Pearl River estuary to the deepwater area (Fig. 1). Seawater samples were collected with Niskin bottles attached to a Rosette sampler. Samples for $\delta^{30}Si_{Si(OH)_4}$ and $Si(OH)_4$ concentration analyses were obtained by filtering 250–500 mL of seawater through 0.45 μm nitrocellulose acetate filters into acid pre-cleaned polyethylene bottles. $\delta^{30}Si_{Si(OH)_4}$ samples were subsequently acidified to pH~2 with distilled concentrated HCl (0.1% v/v) and stored at room temperature in the dark, while $Si(OH)_4$ concentrations were analyzed onboard immediately. Samples for $\delta^{30}Si_{BSi}$ and BSi analyses were obtained by filtering 2–6 L of seawater through 0.4 μm polycarbonate membranes. The membranes were dried at 50 °C overnight and stored in polycarbonate dishes for analysis in the home laboratory. Note that diatoms (~10^3 cell L^{-1}; Chen, 2005) are generally four orders of magnitude more abundant than radiolarians (~10^2 ind. m^{-3}; Wang et al., 2005) in the NSCS. $\delta^{30}Si_{BSi}$ data obtained in this study thus mainly reflect the isotopic compositions of bulk diatoms as the dominant BSi producer in the SCS. In addition, four Pearl River water samples were collected on June 16 before the summer cruise by filtering 250 mL of surface waters through 0.45 μm nitrocellulose acetate filters, in order to

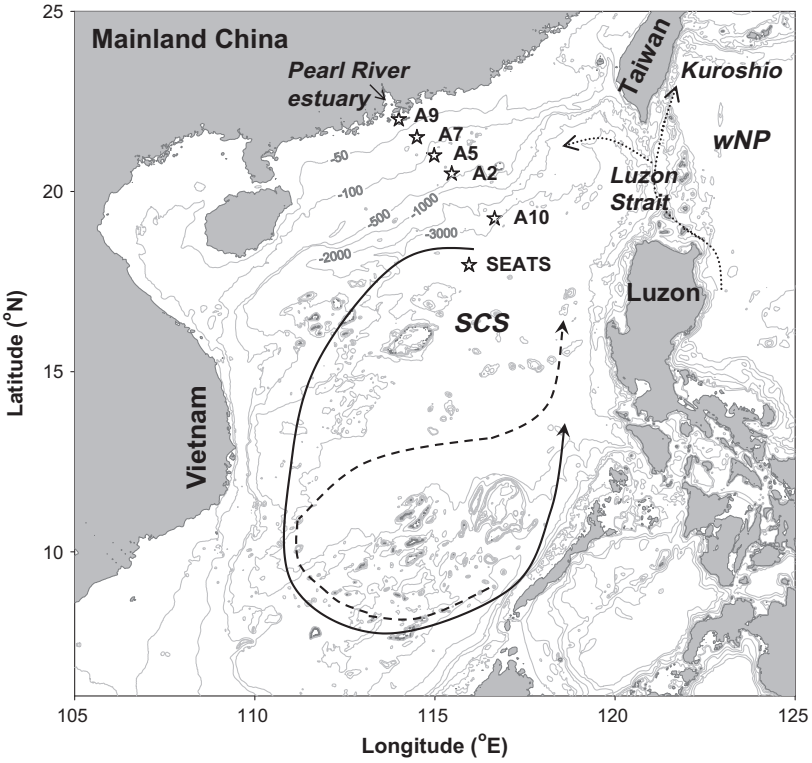

Fig. 1. Map of the South China Sea (SCS) showing its topography and the locations of the sampling stations. The basin scale circulation pattern is according to Wong et al. (2007, and references therein), showing a basin wide cyclonic gyre in winter (solid line) and an anticyclonic gyre over the southern half of the SCS in summer (dashed line). Also shown schematically are the Kuroshio current and its intrusions into the northern SCS around the Luzon Strait (dotted line) according to Wong et al. (2007, and references therein). wNP: the western North Pacific; SEATS: the South East Asian Time-series Study station.

determine the river end-member values of both $\delta^{30}Si_{Si(OH)_4}$ and $Si(OH)_4$ concentrations.

2.2.2. Si isotope analysis

The dissolved $Si(OH)_4$ in the seawater samples was separated from the major matrix elements using a two-step brucite-coprecipitation technique adapted by de Souza et al. (2012) from the MAGIC method (Karl and Tien, 1992). The first precipitate was obtained at a pH of ~10 by adding slightly more than 1.1% by volume of 1 M NaOH. After centrifuging, further addition of 1 M NaOH corresponding to 1.1% by volume was carried out to form more $Mg(OH)_2$ precipitate. After removing the supernatant, the precipitates were dissolved in small amounts of 6 M HCl and diluted with Milli-Q water to a Si concentration of ~1.8 ppm. Through application of this technique, the low $Si(OH)_4$ content in the surface water samples was pre-concentrated by at least a factor of 30, whereas for deep waters with high $Si(OH)_4$ concentrations, only ~5 mL of seawater were required for analysis. Given that near 100% of the dissolved $Si(OH)_4$ was removed from the seawater samples by this treatment, no fractionation affecting the final $\delta^{30}Si_{Si(OH)_4}$ results occurred during the coprecipitation (Cardinal et al., 2005; Reynolds et al., 2006). Due to the much lower amount of matrix elements, river water samples were directly diluted with Milli-Q water to a Si concentration of ~1.8 ppm without the treatment with the brucite-coprecipitation technique (Georg et al., 2006a).

For $\delta^{30}Si_{BSi}$ the particulate samples were dissolved using the first step of the wet-alkaline digestion method developed by Ragueneau et al. (2005), i.e., reaction of 4 mL of 0.2 M NaOH at 100 °C for 40 min. To check for possible lithogenic silica (LSi) contamination, aluminium (Al) concentrations in the solution of digested suspended particles were analyzed using an Agilent 7700 quadrupole-Inductively Coupled Plasma (ICP)-Mass Spectrometer (MS). Significant Al contents representing >10% of the LSi in the sample solution were detected in digested samples from stations A9 and A7 located on the inner shelf. Assuming a $\delta^{30}Si$ of $-0.5‰$ for clays (Douthitt, 1982) and of $+1.5‰$ for diatoms according to De La Rocha et al. (2000) (note that this diatom isotopic signature agrees well with the average $\delta^{30}Si_{BSi}$ of $+1.3‰$ of all our particulate samples), we estimated that the interference in the Si isotope signals introduced by >10% of the LSi would be >0.2‰, which is near our analytical error for $\delta^{30}Si$ determination. As a consequence, the measured $\delta^{30}Si$ for suspended particle samples at stations A9 and A7 were not deemed to be reliable isotopic compositions of BSi and are not shown or discussed in this study. The Al concentrations at the other stations were below the detection limit of ~0.1 ppb, implying nearly zero LSi content in the solutions of the BSi digestions. The contribution of LSi, if existent, was thus too low to contaminate the $\delta^{30}Si_{BSi}$ of suspended particles in offshore waters in the NSCS (Cardinal et al., 2007; Fripiat et al., 2011b).

The Si in the chemically treated solutions of river water, seawater and particulate samples was further purified by an ion-exchange chromatography procedure adapted from Georg et al. (2006b). Typically 1 mL of sample solution with a Si concentration of ~1.8 ppm was loaded onto 1 mL of acid pre-cleaned cation-exchange resin (BioRad AG50W-X8) for complete removal of cations such as magnesium (Mg) and/or sodium (Na), followed by elution with 2 mL of Milli-Q water to ensure 100% Si yields. In the case of surface water samples with low $Si(OH)_4$ concentrations, 2 mL of resin were needed because the large volume (20–30 mL) of samples used for the chemical treatment contained more Mg content. Note that anions were not intentionally removed through the entire chemical procedure given that they are demonstrated to produce no significant offset of the measured Si isotopic compositions (Georg et al., 2006b). We also consider any effect originating from the presence of anions to the suppression of signal intensities (Hendry et al., 2010) negligible during our measurements, due to the fact that the reproducibility of the isotopic compositions of repeat samples were very good (Table 1) and the sample data on a $\delta^{30}Si$ versus $\delta^{29}Si$ plot displayed a well defined linear relationship ($r = 0.98$, $n = 99$) with a slope of 1.91 ± 0.04 (1 standard deviation (SD), $n = 99$) comparable to the theoretical conversion factor of 1.96 assuming a kinetic fractionation law (Young et al., 2002).

$\delta^{30}Si$ values were determined on a Nu Plasma Multi-collector (MC)-ICP-MS (Georg et al., 2006b; Abraham et al., 2008) at GEOMAR, Kiel in dry plasma mode achieved by using a Cetac Aridus II desolvator equipped with a PFA nebulizer with an uptake rate of ~60–80 μL min^{-1}. A standard-sample-standard bracketing technique following Albarède et al. (2004) was employed to obtain the $\delta^{30}Si$ values and all results were given in ‰ deviations relative to the international Si standard NBS28 ($\delta^{30}Si = [(^{30}Si/^{28}Si)_{sample}/(^{30}Si/^{28}Si)_{NBS28} - 1] \times 1000$). The ^{30}Si beam was determined simultaneously with ^{29}Si and ^{28}Si in a pseudo high-resolution mode by determining the isotopic compositions off the centre at the low mass side of the peak top before the $^{14}N^{16}O^+$ interference appeared. 2 mL of a single sample solution with a Si concentration of ~0.6 ppm was usually measured three to five times with a ^{28}Si signal of ~5 V, reaching a sensitivity of ~8 V/ppm while the ^{28}Si blank signal was ~30 mV as obtained by a 2% distilled HNO_3 washing solution. In this context, a total of only ~1 μg of Si is needed to be introduced into the MC-ICP-MS to obtain the $\delta^{30}Si$ value of each sample, which represents the average of the repeated standard bracketing measurements. The small loading sample size, which is more than one order of magnitude less than required by the IRMS method (Brzezinski et al., 2006), allows us to substantially decrease the volume of seawater filtered to obtain sufficient amounts of BSi for the $\delta^{30}Si_{BSi}$ analysis. Repeated measurements of the standard reference materials IRMM-018, Diatomite and Big Batch gave average $\delta^{30}Si$ values of -1.58 ± 0.12‰ (2 SD, $n = 38$), $+1.07 \pm 0.30$‰ (2 SD, $n = 15$) and -10.63 ± 0.24‰ (2 SD, $n = 33$), which agree well with the values obtained during an inter-laboratory comparison experiment (Reynolds et al., 2007). The coupled $\delta^{29}Si$ and $\delta^{30}Si$ data of the three standard reference materials displayed a very well defined linear relationship ($r = 0.9996$, $n = 86$) and the slope of the linear regression line was 0.5089 ± 0.0016 (1 SD, $n = 86$) which is nearly the same as the theoretical kinetic Si isotope fractionation of 0.5092 (Reynolds et al., 2007). The external reproducibility for the replicate measurements of in-house matrix standard over longer periods of time was better than ±0.3‰ (2 SD). Individual error bars of the measured samples provided in this contribution represent 2 SD of repeated standard bracketing measurements of the same sample solution (Table 1).

2.2.3. Analysis of other parameters

Depth profiles of temperature and salinity were determined shipboard with a calibrated SBE-19-plus Conductivity-Temperature-Depth (CTD) recorder (Sea-Bird Co.) attached to the Rosette sampler. $Si(OH)_4$ concentration data were collected onboard using a Technicon AA3 Auto-Analyzer (Bran-Luebbe, GmbH Co.) according to classical colorimetric methods (Han et al., 2012, and references therein). The precision of the $Si(OH)_4$ concentration measurements was within ±3% (1 SD) (Han et al., 2012). In order to analyze the concentrations of BSi deposited on the membranes, the second step of the wet-alkaline digestion (again 4 mL of 0.2 M NaOH at 100 °C for 40 min) was employed and BSi concentrations were calculated by $[BSi] = [Si]_1 - [Al]_1 \times Si/Al)_2$. $[Si]_1$ and $[Al]_1$ denote Si and Al concentrations in the solution of the first digestion. $(Si/Al)_2$ is the ratio obtained in the solution of the second digestion, which is characteristic of the silicate minerals present in the sample as all the BSi dissolves during the first digestion step (Ragueneau et al., 2005). Al concentrations were measured by quadrupole-ICP-MS with a precision of ±1% (1 SD), while Si concentrations were determined on a Technicon AA3 Auto-Analyzer.

3. RESULTS

3.1. $\delta^{30}Si$ distribution along transect A

As shown by the salinity profiles, stations A9, A7 and A5 on the NSCS shelf were well mixed in winter but strongly stratified in summer (Fig. 2). Correspondingly, both $\delta^{30}Si_{Si(OH)_4}$ and $Si(OH)_4$ values were nearly constant through the entire water column in winter, whereas in summer $\delta^{30}Si_{Si(OH)_4}$ generally decreased and $Si(OH)_4$ increased with depth (Fig. 2; Table 1). Although surface $Si(OH)_4$ concentrations were twice as high in winter as in summer, a seasonal $\delta^{30}Si_{Si(OH)_4}$ variation in the surface waters at station A9 was not detected outside analytical error. Significant differences in $\delta^{30}Si_{Si(OH)_4}$ between summer and winter were only observed in the near-bottom waters at stations A7 and A5, where the summer values were lower than in winter and coincided with higher $Si(OH)_4$ concentrations (Fig. 2; Table 1). At stations A2 and A10 respectively located on the NSCS upper and deep-water slope, $\delta^{30}Si_{Si(OH)_4}$ displayed no significant seasonal variations and generally decreased with depth within the water column despite the fact that $Si(OH)_4$ concentrations were overall lower in win-

Table 1
Salinity, silicic acid ($Si(OH)_4$) and biogenic silica (BSi) concentrations and their stable silicon isotopic composition ($\delta^{30}Si_{Si(OH)_4}$ and $\delta^{30}Si_{BSi}$) data collected during the summer and winter cruises to the northern South China Sea (NSCS) in July–August 2009 and January 2010. Also included are salinity, $Si(OH)_4$ and $\delta^{30}Si_{Si(OH)_4}$ data collected during a summer cruise to the Pearl River in June 2009.

Cruise	Station	Depth (m)	Salinity	$Si(OH)_4$ (μmol L^{-1})	$\delta^{30}Si_{Si(OH)_4}$ (‰ ± 2SD[c])	n[a]	BSi (μmol L^{-1})	$\delta^{30}Si_{BSi}$ (‰ ± 2SD[c])	n[a]	$\Delta^{30}Si$[b] (‰ ± 2SD[c])
The Pearl River Summer 2009	P2[d]	Surface	0.18	144.8	1.35 ± 0.26	4				
	P11[d]	Surface	1.46	124.4	1.55 ± 0.30	3				
	P14 [d]	Surface	3.16	115.9	1.23 ± 0.25	4				
	P17[d]	Surface	3.98	109.5	1.49 ± 0.29	3				
NSCS Summer 2009	A9	6.0	31.55	4.4	2.41 ± 0.28	4				
	22.0°N	16.3	32.72	5.7						
	114.0°E	30.8	33.79	9.4	1.81 ± 0.24	3				
	A7	4.9	33.62	1.6	2.58 ± 0.12	4				
	21.5°N	25.9	33.82	1.7	2.94 ± 0.26	5				
	114.5°E	51.5	34.24	4.9	2.15 ± 0.17	4				
		68.5	34.34	8.4	1.85 ± 0.33	5				
	A5	5.5	33.52	1.5	2.51 ± 0.21	4				
	21.0°N	26.4	33.58	1.6						
	115.0°E	50.5	33.80	2.1	2.39 ± 0.28	4				
		75.9	34.12	5.0						
		94.8	34.43	12.4	1.72 ± 0.23	4				
	A2	5.3	33.46	2.1	2.74 ± 0.23	4	0.04	1.63 ± 0.22	4	−1.11 ± 0.32
	20.5°N	25.5	33.45	1.9						
	115.5°E	50.0	33.93	2.9	2.55 ± 0.25	4	0.07	1.14 ± 0.19	4	−1.41 ± 0.31
		74.7	34.33	9.6						
		97.9	34.47	13.3	1.75 ± 0.16	4	0.12	−0.17 ± 0.25	4	−1.92 ± 0.30
		148.9	34.55	18.8			0.14	0.14 ± 0.13	4	
		199.6	34.50	15.7	1.66 ± 0.19	4				
		298.9	34.44	41.9	1.48 ± 0.17	4				
		298.9	Duplicate		1.30 ± 0.25	3				
		367.9	34.43	50.3						
	A10	5.3	33.40	1.7	2.71 ± 0.20	4	0.02	1.36 ± 0.25	3	−1.35 ± 0.32
	19.2°N	48.9	33.87	2.9	2.36 ± 0.11	4	0.07	−0.70 ± 0.25	4	−3.06 ± 0.28
	116.7°E	74.7	34.15	7.9						
		99.5	34.38	12.3	1.71 ± 0.26	4	0.05	1.10 ± 0.36	4	−0.61 ± 0.44
		99.5	Duplicate		1.99 ± 0.18	3				
		124.6	34.54	15.3						
		149.0	34.55	17.2						
		198.8	34.52	25.6	1.62 ± 0.20	4	0.04	1.20 ± 0.11	4	−0.42 ± 0.23
		298.7	34.46	41.2						
		497.6	34.42	66.7	1.56 ± 0.30	3	0.04	1.03 ± 0.08	4	−0.53 ± 0.31
		497.6	Duplicate		1.43 ± 0.32	4				
		793.0	34.47	101.2						
		991.5	34.51	118.2	1.27 ± 0.27	3				
		1485.4	34.58	128.6						
		1978.3	34.60	143.2	0.96 ± 0.21	3				
		2469.7	34.61	144.8						
	SEATS[e]	7.1	33.25	1.6	2.88 ± 0.34	4	0.02	2.61 ± 0.13	4	−0.27 ± 0.37
	18.0°N	27.0	33.25	1.6	2.33 ± 0.19	4	0.03	2.36 ± 0.08	4	0.03 ± 0.21
	116.0°E	50.6	34.06	4.9	2.24 ± 0.16	4	0.07	1.37 ± 0.16	4	−0.87 ± 0.22
		100.0	34.39	12.8	1.33 ± 0.36	4	0.03	2.18 ± 0.31	3	0.85 ± 0.47
		149.4	34.54	20.7	1.60 ± 0.11	4	0.03	2.07 ± 0.10	4	0.47 ± 0.15
		200.6	34.54	24.9	1.15 ± 0.20	5	0.03	1.95 ± 0.41	4	0.80 ± 0.46
		496.8	34.42	60.6	1.53 ± 0.34	3	0.03	1.95 ± 0.16	4	0.42 ± 0.38
		793.7	34.47	99.8	1.03 ± 0.20	5				
		993.0	34.51	106.0	0.95 ± 0.23	5				
		1978.0	34.60	138.6	0.81 ± 0.28	5				

(*continued on next page*)

Table 1 (*continued*)

Cruise	Station	Depth (m)	Salinity	$Si(OH)_4$ ($\mu mol\ L^{-1}$)	$\delta^{30}Si_{Si(OH)_4}$ (‰ ± 2SD[c])	n[a]	BSi ($\mu mol\ L^{-1}$)	$\delta^{30}Si_{BSi}$ (‰ ± 2SD[c])	n[a]	$\Delta^{30}Si$[b] (‰ ± 2SD[c])
		2981.4	34.61	147.5	0.93 ± 0.15	4				
NSCS Winter 2009	A9	5.9	32.40	9.3	2.19 ± 0.34	3				
	22.0°N	15.6	32.41	9.2						
	114.0°E	30.1	32.51	9.3	2.11 ± 0.31	4				
	A7	4.8	34.28	1.7	2.41 ± 0.10	4				
	21.5°N	25.7	34.28	1.7	2.51 ± 0.17	5				
	114.5°E	48.8	34.14	1.6	2.62 ± 0.13	4				
		67.8	34.10	1.6	2.71 ± 0.36	5				
	A5	5.9	34.41	1.0	2.41 ± 0.16	4	0.19	0.63 ± 0.17	4	−1.78 ± 0.23
	21.0°N	25.4	34.41	1.0						
	115.0°E	51.1	34.45	1.2	2.27 ± 0.24	4	0.26	0.30 ± 0.15	4	−1.97 ± 0.28
		73.0	34.42	1.3						
		96.0	34.41	1.9	2.38 ± 0.28	4	0.22	0.28 ± 0.11	4	−2.10 ± 0.31
	A2	3.1	34.17	1.1	2.54 ± 0.30	4	0.28	0.64 ± 0.17	4	−1.90 ± 0.34
	20.5°N	24.2	34.16	1.1						
	115.5°E	47.6	34.26	1.3	2.37 ± 0.20	4	0.50	0.65 ± 0.23	4	−1.72 ± 0.31
		73.3	34.30	1.5						
		99.2	34.57	4.8	1.98 ± 0.13	4	0.19	0.93 ± 0.19	4	−1.05 ± 0.23
		122.9	34.66	7.9						
		149.5	34.67	8.3			0.09	0.90 ± 0.11	4	
		198.4	34.58	14.2	1.46 ± 0.26	4				
		298.4	34.46	30.0	1.40 ± 0.15	4				
		298.4	Duplicate		1.50 ± 0.30	3				
	A10	6.2	33.80	1.7	2.48 ± 0.23	4	0.17	0.83 ± 0.14	4	−1.65 ± 0.27
	19.2°N	25.2	33.80	1.7						
	116.7°E	50.1	33.82	1.6	2.61 ± 0.14	4	0.17	1.00 ± 0.14	4	−1.61 ± 0.20
		75.6	34.29	1.2						
		99.1	34.41	6.2	1.94 ± 0.20	4	0.14	0.68 ± 0.33	4	−1.26 ± 0.38
		125.0	34.49	8.5						
		150.1	34.65	8.5						
		198.6	34.55	14.7	1.48 ± 0.36	4	0.10	0.64 ± 0.16	4	−0.84 ± 0.39
		300.2	34.44	36.9						
		499.7	34.41	63.4	1.41 ± 0.23	4	0.11	1.03 ± 0.19	4	−0.38 ± 0.29
		799.3	34.46	92.5						
		998.9	34.51	111.7	1.23 ± 0.30	3				
	SEATS[e]	6.6	33.72	2.4	2.87 ± 0.34	5	0.08	2.79 ± 0.34	3	−0.08 ± 0.48
	18.0°N	25.8	33.74	2.4	2.48 ± 0.23	4	0.08	2.42 ± 0.32	4	−0.06 ± 0.39
	116.0°E	50.4	33.86	5.6	1.85 ± 0.24	5	0.05	2.41 ± 0.24	3	0.56 ± 0.35
		50.4	Duplicate		1.91 ± 0.22	4				
		98.5	34.52	10.5	1.41 ± 0.15	4	0.09	2.04 ± 0.23	4	0.63 ± 0.27
		151.6	34.59	13.0	1.63 ± 0.18	4	0.08	2.33 ± 0.18	4	0.70 ± 0.26
		199.4	34.52	22.1	1.40 ± 0.25	5	0.07	2.45 ± 0.26	4	1.05 ± 0.36
		499.6	34.42	67.9	1.49 ± 0.29	4	0.03	2.73 ± 0.19	4	1.24 ± 0.35
		800.6	34.48	98.8	1.19 ± 0.29	5				
		1000.2	34.52	113.1	1.09 ± 0.19	5				
		2000.4	34.60	135.4	0.94 ± 0.26	5				
		2999.7	34.61	135.3	1.05 ± 0.21	5				
		2999.7	Duplicate		1.06 ± 0.17	4				

[a] n is the number of the repeated standard bracketing measurements for $\delta^{30}Si$ of a single sample solution.

[b] $\Delta^{30}Si$ is the apparent fractionation factor defined as the difference between $\delta^{30}Si_{BSi}$ and $\delta^{30}Si_{Si(OH)_4}$ (Eq. (7)).

[c] SD is the standard deviation estimated from the repeated standard bracketing measurements of a single sample solution.

[d] Locations of the four sampling stations in the Pearl River are P2: 22.8°N, 113.6°E; P11: 22.6°N, 113.8°E; P14: 22.4°N, 113.8°E; and P17: 22.2°N, 113.7°E.

[e] SEATS is abbreviation of the South East Asian Time-series Study station established in the NSCS basin.

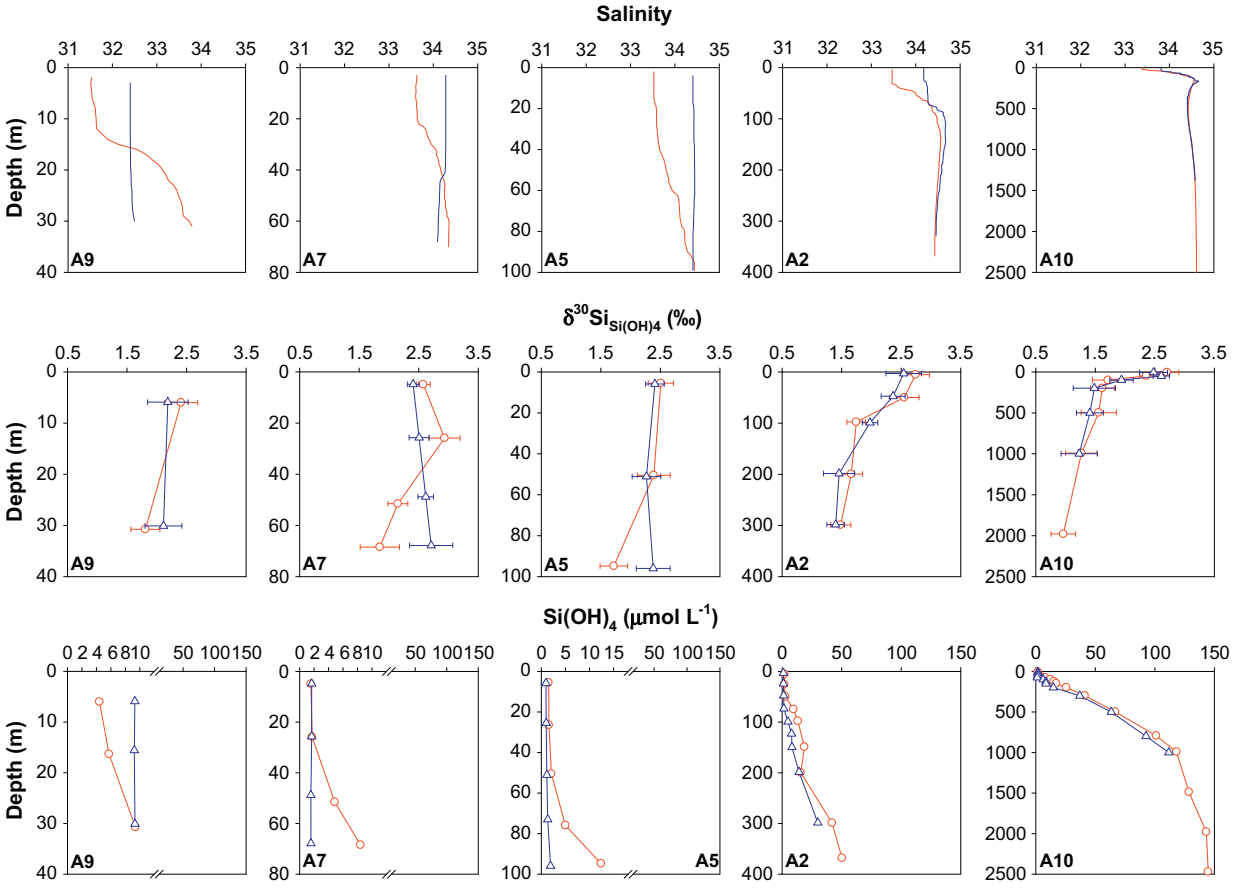

Fig. 2. Vertical distributions of (top) salinity, (middle) $\delta^{30}Si_{Si(OH)_4}$ and (bottom) $Si(OH)_4$ at stations along transect A in summer (red circles and lines) and winter (blue triangles and lines). Error bars of $\delta^{30}Si_{Si(OH)_4}$ in this figure and those of all field $\delta^{30}Si_{Si(OH)_4}$ and $\delta^{30}Si_{BSi}$ data in the following figures represent 2 standard deviations of repeated measurements of the same sample solution. (For interpretation of the references to color in this figure legend, the reader is referred to the web version of this article.)

ter than in summer (Fig. 2; Table 1). Note that the salinity extremes at station A10 (Fig. 2) are influenced by the advection of North Pacific Tropical Water (NPTW) around 150–200 m and North Pacific Intermediate Water (NPIW) around 500 m, respectively (Cao and Dai, 2011, and references therein). Our observed $\delta^{30}Si_{Si(OH)_4}$ at the salinity minimum layer around 500 m was $+1.5 \pm 0.2‰$ (Fig. 2; Table 1), which is indistinguishable from the value of $+1.4 \pm 0.1‰$ for NPIW given by Reynolds et al. (2006).

Due to significant LSi contents in the solution of digested suspended particles from the membranes collected from stations A9 and A7, reliable $\delta^{30}Si_{BSi}$ results were only obtained for the three offshore stations along transect A (Fig. 3; Table 1). No significant vertical gradients of $\delta^{30}Si_{BSi}$ were observed at each station in winter while the corresponding BSi concentrations varied slightly. On the other hand, the summer $\delta^{30}Si_{BSi}$ distributions displayed an approximately inverse relationship with BSi concentrations. At station A2 in summer, $\delta^{30}Si_{BSi}$ decreased while BSi concentrations increased with depth in the upper 100 m. At station A10 in summer, a $\delta^{30}Si_{BSi}$ minimum corresponding to a BSi maximum was observed in waters at 50 m water depth (Fig. 3). $\delta^{30}Si_{BSi}$ values, ranging from $\sim -0.7‰$ to $\sim +1.6‰$, were systematically lower than the corresponding $\delta^{30}Si_{Si(OH)_4}$ at stations A5, A2 and A10 in both seasons, except for the $\delta^{30}Si_{BSi}$ value in deep waters at station A10, which was identical to $\delta^{30}Si_{Si(OH)_4}$ within analytical error (Fig 3; Table 1).

3.2. δ^{30}Si distribution at station SEATS

$\delta^{30}Si_{Si(OH)_4}$ at station SEATS generally decreased with water depth while the $Si(OH)_4$ displayed an overall inverse trend (Fig. 4). No significant $\delta^{30}Si_{Si(OH)_4}$ differences outside analytical error were observed between summer and winter through the entire water column, except that $\delta^{30}Si_{Si(OH)_4}$ in winter at 50 m water depth was slightly lower than during summer ($+1.8 \pm 0.2‰$ versus $+2.2 \pm 0.2‰$; Fig. 4; Table 1). In both seasons, the surface $\delta^{30}Si_{Si(OH)_4}$ values amounted to $+2.9 \pm 0.3‰$ coinciding with the lowest $Si(OH)_4$ concentrations of ~ 2 μmol L^{-1}. $\delta^{30}Si_{Si(OH)_4}$ decreased rapidly from the surface to 100 m depth followed by a further slight decrease from 200 m down to 1000 m water depth. Below 1000 m, the $\delta^{30}Si_{Si(OH)_4}$ values were essentially constant at a value of $\sim +1.0‰$. Correspondingly, $Si(OH)_4$ concentrations increased linearly from the surface to 1000 m and

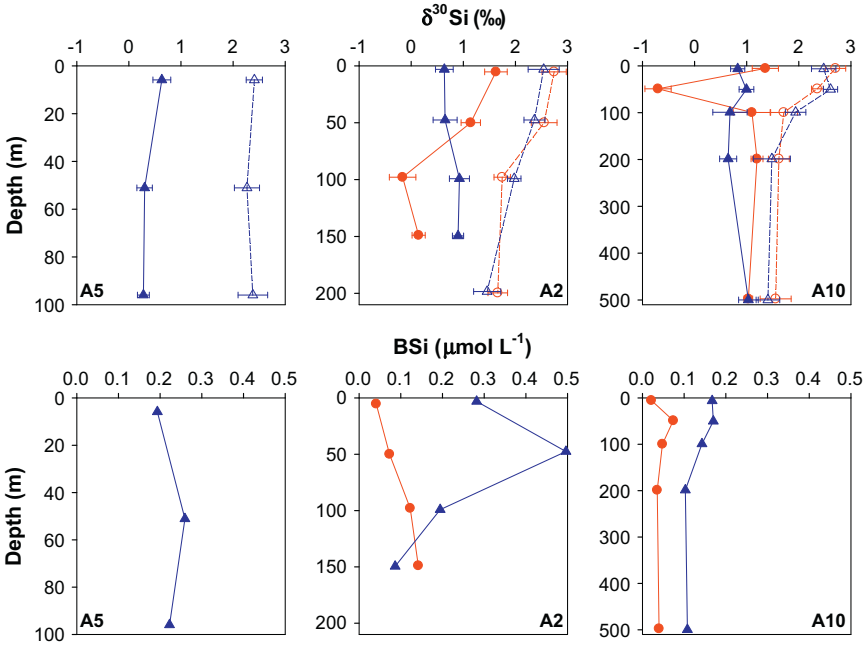

Fig. 3. Vertical distributions of (top) $\delta^{30}Si_{BSi}$ (solid symbols) and $\delta^{30}Si_{Si(OH)_4}$ (open symbols) at stations A5, A2 and A10 in summer (red circles) and winter (blue triangles). At the bottom the corresponding BSi concentrations for both seasons are shown. Note that $\delta^{30}Si_{BSi}$ and BSi data were not available for station A5 in summer. (For interpretation of the references to color in this figure legend, the reader is referred to the web version of this article.)

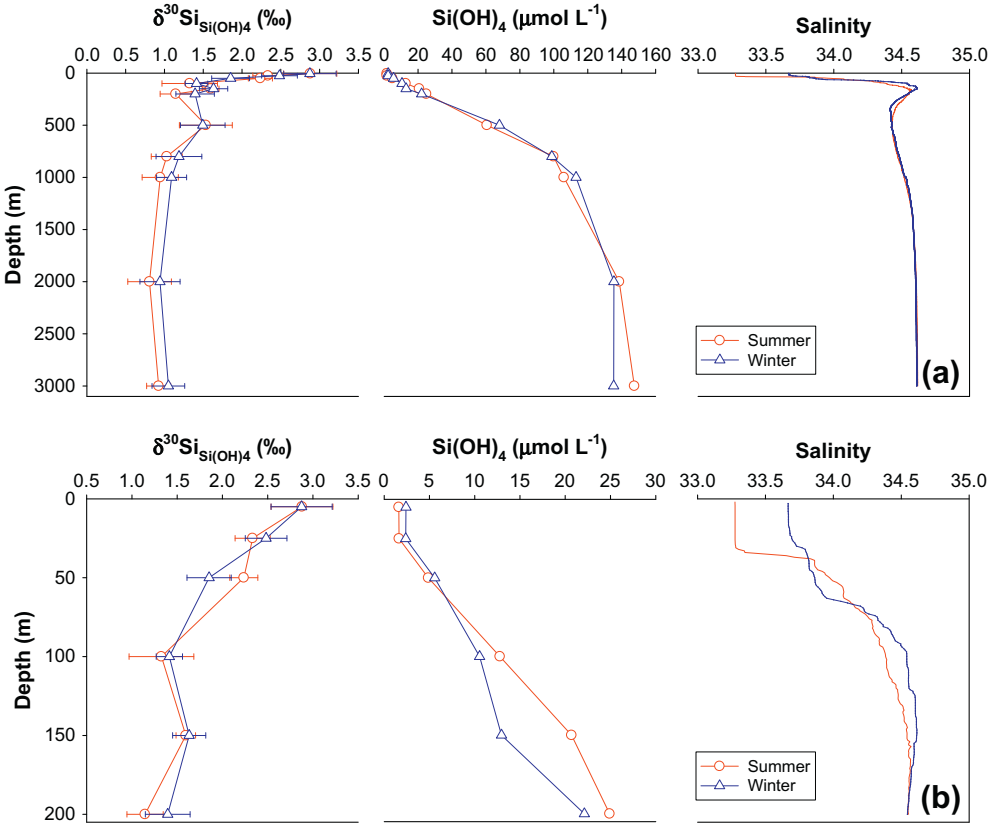

Fig. 4. Vertical distributions of $\delta^{30}Si_{Si(OH)_4}$, $Si(OH)_4$ and salinity in the entire water column (a) and in the upper 200 m of the water column (b) at station SEATS.

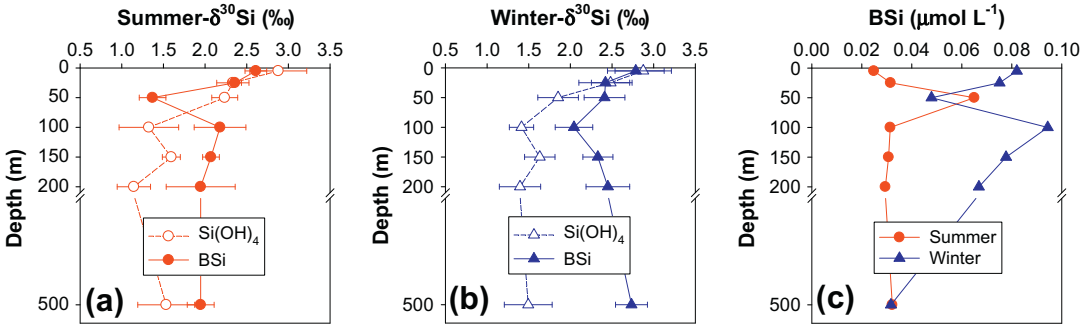

Fig. 5. Vertical distributions of $\delta^{30}Si_{Si(OH)_4}$ and $\delta^{30}Si_{BSi}$ in the upper 500 m of the water column at station SEATS in summer (a) and winter (b). Also shown are corresponding BSi concentrations for both seasons (c).

showed a further increase below 1000 m (Fig. 4). The observed $\delta^{30}Si_{Si(OH)_4}$ for the salinity minimum layer around 500 m at station SEATS was $+1.5 \pm 0.3‰$, which agrees well with that at station A10 (Table 1).

BSi concentrations in the upper 500 m of the water column at station SEATS were lower than 0.1 μmol L^{-1}, which were less than half of those found at stations along transect A while the maximum value at station A2 in winter (Fig. 3; Table 1) was even five times higher than that at station SEATS (Fig. 5c; Table 1). The net BSi production in the oligotrophic basin is thus significantly lower than that in the shelf and slope areas of the NSCS. Although the BSi concentrations in winter were generically higher than those in summer, $\delta^{30}Si_{BSi}$ values in winter were overall comparable to those in summer while an apparent small difference was only observed in waters at 50 m depth. Within analytical error, vertical $\delta^{30}Si_{BSi}$ distributions in both seasons displayed only minor variations within the upper 500 m of the water column at station SEATS although in the summer profile a significantly lower $\delta^{30}Si_{BSi}$ value of $+1.4 \pm 0.2‰$ was observed in waters at 50 m corresponding to the maximum BSi concentration of ~0.07 μmol L^{-1} (Fig. 5; Table 1). A closer look at the $\delta^{30}Si_{Si(OH)_4}$ and $\delta^{30}Si_{BSi}$ profiles at station SEATS reveal that the $\delta^{30}Si_{BSi}$ was either equal to or higher than the corresponding $\delta^{30}Si_{Si(OH)_4}$ in the upper 500 m of the water column (Fig. 5a and b). The exception to this feature is that the $\delta^{30}Si_{BSi}$ value was significantly lower than $\delta^{30}Si_{Si(OH)_4}$ at 50 m in summer (Fig. 5a). Note that a number of previous studies (Varela et al., 2004; Cardinal et al., 2007; Cavagna et al., 2011; Fripiat et al., 2011b) as well as our observations in the shelf and slope areas of the NSCS did observe systematically lower $\delta^{30}Si_{BSi}$ than $\delta^{30}Si_{Si(OH)_4}$ in surface waters as expected from the preferential uptake of lighter Si isotopes by diatoms.

4. DISCUSSION

Stations along transect A, besides station SEATS, were investigated under changing hydrographic conditions in the NSCS where various water masses contribute to its upper layer. On the other hand, all of our surface samples displayed the heaviest $\delta^{30}Si_{Si(OH)_4}$ value with the overall increasing trend from nearshore to offshore waters (Figs. 2 and 4; Table 1), suggesting variable biological utilization among different regimes. In this section, upon a summary of the natural range of oceanic $\delta^{30}Si$, we present the Si isotope fractionation models. Subsequently, we examine the physical and biological processes in controlling the $\delta^{30}Si$ dynamics in different regimes of the NSCS.

4.1. Natural range of oceanic $\delta^{30}Si_{Si(OH)_4}$ and $\delta^{30}Si_{BSi}$

On the basis of the up to date Si isotopic composition data reported for the world's oceans and seas, $\delta^{30}Si_{Si(OH)_4}$ and $\delta^{30}Si_{BSi}$ display the largest variability in surface waters while both variations generally decrease with depth (Fig. 6). Below 3000 m of various oceanic regimes, $\delta^{30}Si_{Si(OH)_4}$ values tend to converge to a constant value of $+0.9‰$ except in the Equatorial Pacific Deep Water (EPDW; Beucher et al., 2008, 2011) which are significantly heavier. The global dissolved seawater $\delta^{30}Si_{Si(OH)_4}$ ranges from $+0.5‰$ to $+3.2‰$ through the entire water column, with the lowest value observed for the North Pacific Deep Water (NPDW; Reynolds et al., 2006) and the highest values occurring in the surface North Pacific (Reynolds et al., 2006) and Southern Ocean (Fripiat et al., 2011a). $\delta^{30}Si_{Si(OH)_4}$ values of the NSCS varied between $+0.9‰$ and $+2.9‰$, which is within the $\delta^{30}Si_{Si(OH)_4}$ range reported for the North Pacific (Reynolds et al., 2006) (Fig 6a). On the other hand, $\delta^{30}Si_{BSi}$ of suspended particles in the NSCS upper water column varied within a range from $-0.7‰$ to $+2.8‰$, which is slightly larger than that from $-0.5‰$ to $+2.6‰$ in the Southern Ocean. The ranges of $\delta^{30}Si_{BSi}$ at each depth between 100 m and 500 m in the NSCS are comparable to those in the Southern Ocean (Fig. 6b).

4.2. Modeling Si isotope fractionation during $Si(OH)_4$ utilization

Si isotope fractionation during $Si(OH)_4$ utilization by diatoms can be described by a Rayleigh or a steady state model (Fripiat et al., 2011b, and references therein). The Rayleigh model assumes a closed system with no further supply of nutrients from external sources, which is illustrated by the following equations:

$$\delta^{30}Si_{Si(OH)4} = \delta^{30}Si_{Si(OH)4\_initial} + {}^{30}\varepsilon_{upt} \times \ln(f) \quad (1)$$

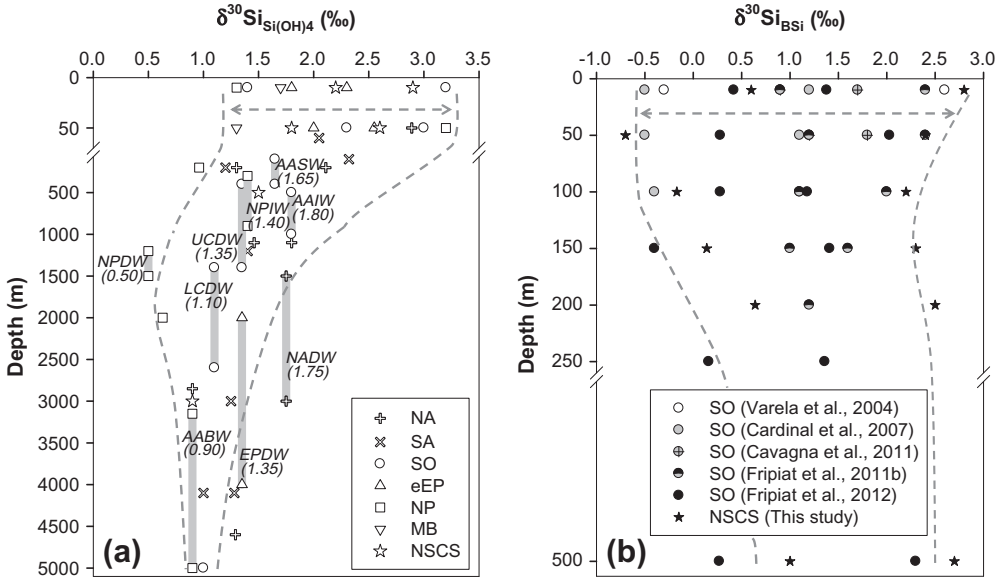

Fig. 6. (a) Range of $\delta^{30}Si_{Si(OH)_4}$ in the world's oceanic waters. Data of the North Atlantic (NA) and the South Atlantic (SA) are from De La Rocha et al. (2000) and de Souza et al. (2012). Data of the Southern Ocean (SO) are from Varela et al. (2004), Cardinal et al. (2005), Cavagna et al. (2011), De La Rocha et al. (2011) and Fripiat et al. (2011a, 2011b). Data of the eastern Equatorial Pacific (eEP) are from Beucher et al. (2008, 2011). Data of the North Pacific (NP) are from De La Rocha et al. (2000) and Reynolds et al. (2006). Data of the Monterey Bay (MB) are from De La Rocha et al. (2000). Also shown are $\delta^{30}Si_{Si(OH)_4}$ data of the northern South China Sea (NSCS) from this study and $\delta^{30}Si_{Si(OH)_4}$ values for several typical water masses around the world's ocean. NADW: North Atlantic Deep Water (de Souza et al., 2012); AASW: Antarctic Surface Water (Fripiat et al., 2011a, 2011b); AAIW: Antarctic Intermediate Water (Fripiat et al., 2011a); UCDW: Upper Circumpolar Deep Water (Fripiat et al., 2011a, 2011b); LCDW: Lower Circumpolar Deep Water (Fripiat et al., 2011b); AABW: Antarctic Bottom Water (Reynolds et al., 2006); EPDW: Equatorial Pacific Deep Water (Beucher et al., 2008, 2011); NPIW: North Pacific Intermediate Water (Reynolds et al., 2006) and NPDW: North Pacific Deep Water (Reynolds et al., 2006). (b) Range of $\delta^{30}Si_{BSi}$ in the upper 500 m of the water column in the Southern Ocean and the northern South China Sea. Note that the measured $\delta^{29}Si$ data from Cardinal et al. (2005, 2007) were converted into $\delta^{30}Si$ by multiplication with the theoretical conversion factor of 1.96 assuming a kinetic fractionation law (Young et al., 2002) and only employed were $\delta^{30}Si$ data outside the iron fertilized patch in the study of Cavagna et al. (2011).

$$\delta^{30}Si_{BSi\_inst} = \delta^{30}Si_{Si(OH)4} + {}^{30}\varepsilon_{upt} \quad (2)$$

$$\delta^{30}Si_{BSi\_acc} = \delta^{30}Si_{Si(OH)4\_initial} - {}^{30}\varepsilon_{upt} \times \frac{f \times \ln(f)}{1-f} \quad (3)$$

$$f = \frac{[Si(OH)_4]_{observed}}{[Si(OH)_4]_{initial}} \quad (4)$$

The subscript "initial" denotes $\delta^{30}Si_{Si(OH)_4}$ and $Si(OH)_4$ values prior to biological utilization. The term f indicates the fraction of remaining dissolved $Si(OH)_4$ in solution relative to the initial concentration at any given time. The subscripts "inst" and "acc" denote instantaneous BSi and accumulated BSi, respectively.

Alternatively, the steady state model describes the evolution of $\delta^{30}Si_{Si(OH)_4}$ (Eq. (5)) and $\delta^{30}Si_{BSi}$ (Eq. (6)) by assuming an open system with continuous supply of nutrients:

$$\delta^{30}Si_{Si(OH)4} = \delta^{30}Si_{Si(OH)4\_initial} - {}^{30}\varepsilon_{upt} \times (1-f) \quad (5)$$

$$\delta^{30}Si_{BSi} = \delta^{30}Si_{Si(OH)4\_initial} + {}^{30}\varepsilon_{upt} \times f = \delta^{30}Si_{Si(OH)4} + {}^{30}\varepsilon_{upt} \quad (6)$$

The apparent fractionation factor defined as $\Delta^{30}Si$ (Eq. (7)) is the difference between the observed isotopic compositions of the BSi product and the $Si(OH)_4$ substrate (Cardinal et al., 2007; Cavagna et al., 2011). Assuming that no BSi accumulation occurs in the system, $\Delta^{30}Si$ equals ${}^{30}\varepsilon_{upt}$ in the steady state model, as well as in the Rayleigh model where $\delta^{30}Si_{BSi}$ represents the isotopic composition of instantaneously formed BSi (Eq. (2)).

$$\Delta^{30}Si = \delta^{30}Si_{BSi} - \delta^{30}Si_{Si(OH)4} \quad (7)$$

In this study, field data are compared with calculated values from both models in order to validate the $Si(OH)_4$ sources for diatom growth in different areas of the NSCS.

4.3. Biological fractionation and the Pearl River input of $Si(OH)_4$ in surface waters of the NSCS inner shelf

The lowest surface salinity of ~31.5 was observed at station A9 on the inner shelf in summer along with the highest summer surface $Si(OH)_4$ of ~4.4 μmol L^{-1} (Fig. 2; Table 1) documenting significant freshwater inputs from the Pearl River. Such low salinity waters were produced by estuarine mixing between the Pearl River water and the NSCS surface water. Average salinity, $Si(OH)_4$ concentration and $\delta^{30}Si_{Si(OH)_4}$ from the four Pearl River water samples (Table 1) were determined to be 2.2, 124 μmol L^{-1} and $+1.4 \pm 0.1$‰, respectively. On the other hand, salinity, $Si(OH)_4$ concentration and $\delta^{30}Si_{Si(OH)_4}$ values for the NSCS surface water end-member were estimated to be 33.5,

2 μmol L^{-1} and $+2.6 \pm 0.1‰$, respectively, which are averages of summer surface values from stations A7, A5, A2 and A10 (Table 1). Mixing between the two end-member waters to a given salinity of ~31.5 (the summer surface salinity at station A9; Table 1) predicted a $\delta^{30}Si_{Si(OH)_4}$ of $+1.6 \pm 0.1‰$ and a $Si(OH)_4$ concentration of ~9.6 μmol L^{-1}. Assuming $^{30}\varepsilon_{upt} = -1.1 \pm 0.4‰$ (De La Rocha et al., 1997), the subsequent $Si(OH)_4$ utilization to a value of ~4.4 μmol L^{-1} (the summer surface $Si(OH)_4$ concentration at station A9; Table 1) induced a final $\delta^{30}Si_{Si(OH)_4}$ of $+2.5 \pm 0.3‰$ following the Rayleigh model (Eq. (1)) or $+2.2 \pm 0.2‰$ following the steady state model (Eq. (5)). Both values are consistent with the observed surface $\delta^{30}Si_{Si(OH)_4}$ of $+2.4 \pm 0.3‰$ at station A9 in summer (Table 1), indicating that the diatom growth primarily stimulated by the Pearl River input of $Si(OH)_4$ determines $\delta^{30}Si_{Si(OH)_4}$ in the nearshore surface waters of the NSCS.

Note that the Pearl River water samples were collected nearly two months prior to the investigation of station A9 on August 6 (Table 1). Intraseasonal variations of the Pearl River end-member value are possible but should be too small to affect our calculation, given that the Pearl River water discharge rate was overall similar in June and August 2009 (data not shown). In addition, the surface salinity at station A9 in winter was higher but still <33.0 (Fig. 2; Table 1), implying a weaker but still clearly noticeable influence of freshwater input. The lack of the end-member value of $\delta^{30}Si_{Si(OH)_4}$ for the winter Pearl River water, which might vary seasonally, did not allow similar calculations for the winter situation.

4.4. Biological fractionation and vertical mixing of $Si(OH)_4$ on the NSCS outer shelf and slope

4.4.1. Station A5 in winter

The highest surface salinity of ~34.4 was observed at station A5 on the outer shelf in winter (Fig. 2; Table 1), which possibly originated from intrusions from the surface layer of the wNP or the deeper interior of the SCS. Surface waters of the wNP are highly depleted in $Si(OH)_4$ (<1 μmol L^{-1}) reaching $\delta^{30}Si_{Si(OH)_4}$ values >+3.0‰ (Reynolds et al., 2006) which is higher than all surface values observed in the NSCS. Moreover, such an initial condition of extremely low $Si(OH)_4$ concentration is unable to fuel the high BSi production at station A5 in winter relative to that at station SEATS, which induced the significant Si isotope fractionation between $Si(OH)_4$ and BSi in the former case (Fig. 3). Note that surface temperature of ~22.6 °C at station A5 in winter was lower than those at the more offshore stations A10 and SEATS (~24.5 °C), further suggesting that the high salinity waters were unlikely derived from surface waters of the wNP as the Kuroshio surface water is typically warmer (>26 °C; Chern et al., 1990; Qu et al., 2000).

On the other hand, upwelling or mixing events inject $Si(OH)_4$ from the deeper interior of the SCS into the surface layer (Chao et al., 1996; Wong et al., 2007). In particular in winter the monsoon-induced cyclonic gyre (Fig. 1) substantially facilitates the upward movement of the deep water

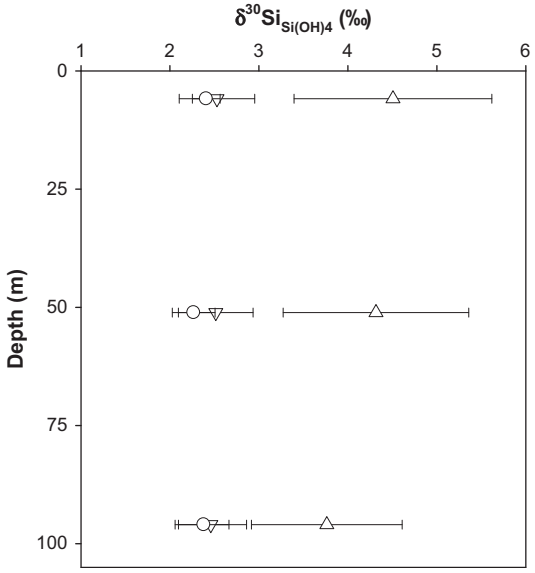

Fig. 7. Vertical distribution of observed $\delta^{30}Si_{Si(OH)_4}$ (circles) and calculated $\delta^{30}Si_{Si(OH)_4}$ following the Rayleigh (up triangles) or the steady state (down triangles) models at station A5 in winter. Note that error bars of the model calculated $\delta^{30}Si_{Si(OH)_4}$ were obtained through the error propagation of both the initial $\delta^{30}Si_{Si(OH)_4}$ value and of $^{30}\varepsilon_{upt}$ given by De La Rocha et al. (1997).

(Qu, 2000). Vertical property distributions at station A5 in winter displayed distinctly homogeneous characteristics (Figs. 2 and 3), suggesting that nutrients in the entire ~100 m water column were supplied from the immediately underlying waters. As no significant seasonal variations of $\delta^{30}Si_{Si(OH)_4}$ were observed in waters below 100 m of the NSCS (Figs. 2 and 4), the average values for $\delta^{30}Si_{Si(OH)_4}$ and $Si(OH)_4$ around the salinity maximum layer (~150–200 m) were estimated to be $+1.5 \pm 0.2‰$ and 15 μmol L^{-1} by the combination of the field data from the two cruises (Table 1). Taking these values as the initial condition and assuming $^{30}\varepsilon_{upt} = -1.1 \pm 0.4‰$ (De La Rocha et al., 1997), the calculated $\delta^{30}Si_{Si(OH)_4}$ following the Rayleigh model (Eq. (1)) were significantly higher than observed through the entire water column at station A5 in winter, whereas for the steady state model (Eq. (5)) the agreement between the calculated and observed $\delta^{30}Si_{Si(OH)_4}$ was very good (Fig. 7). This finding is consistent with the fact that continuous upward supply of nutrients is likely due to either strong upwelling or vertical mixing in the interior of the SCS (Chao et al., 1996; Wong et al., 2007). Although $\delta^{30}Si_{BSi}$ were systematically lower than the corresponding $\delta^{30}Si_{Si(OH)_4}$ at station A5 in winter (Fig. 3), the average $\Delta^{30}Si$ of $-1.9 \pm 0.2‰$ (Eq. (7)) estimated from the three observed values (Table 1) was higher than $-1.1 \pm 0.4‰$ (De La Rocha et al., 1997), which was most likely biased by asynchronous processes setting the $\delta^{30}Si_{BSi}$ and $\delta^{30}Si_{Si(OH)_4}$ signatures. For instance, an export of newly formed diatoms which are isotopically heavier than the older ones may have induced higher $\Delta^{30}Si$ values (Cardinal et al., 2007). Note that a similar average $\Delta^{30}Si$ value of $-1.6‰$ has been observed in the surface waters of the Southern Ocean (Varela et al., 2004). We contend that upwelling or vertical mixing of deep nutrient-rich waters followed by

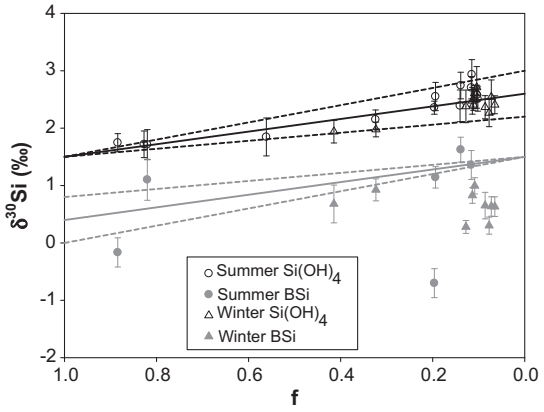

Fig. 8. $\delta^{30}Si_{Si(OH)_4}$ and $\delta^{30}Si_{BSi}$ versus f (f is the fraction of remaining $Si(OH)_4$ relative to the initial concentration; Eq. (4)) for the upper 100 m of the water column along transect A. For the initial condition waters around the salinity maximum layer (~150–200 m) in the northern South China Sea with an average $\delta^{30}Si_{Si(OH)_4}$ of $+1.5 \pm 0.2‰$ and $Si(OH)_4$ of 15 μmol L^{-1} were applied. The solid black and gray lines indicate theoretical $\delta^{30}Si_{Si(OH)_4}$ and $\delta^{30}Si_{BSi}$ evolutions following the steady state model with $^{30}\varepsilon_{upt} = -1.1‰$ (fractionation factor during $Si(OH)_4$ utilization), while the dashed lines above and below indicate errors deduced from the uncertainties of ±0.4‰ in the $^{30}\varepsilon_{upt}$ estimation (De La Rocha et al., 1997). Note that $\delta^{30}Si_{Si(OH)_4}$ data from station A9 were not included due to the clear influence of river inputs.

extensive utilization of $Si(OH)_4$ in an open system best explains the $\delta^{30}Si$ patterns observed at station A5 in winter.

4.4.2. The upper 100 m of the water column along transect A

The $\delta^{30}Si_{BSi}$ was systematically lower than the corresponding $\delta^{30}Si_{Si(OH)_4}$ in the upper 100 m of the water column at stations A5, A2 and A10 (Fig. 3), despite that $\Delta^{30}Si$ values varied within a large range between −3.0‰ and −0.6‰ (Table 1). In those NSCS shelf and slope areas without important riverine inputs, the expected primary nutrient source of the euphotic zone (mostly extending from the surface to ~75–100 m water depth in the SCS; Liu et al., 2001) are the underlying waters, either through upwelling or mixing between surface and deeper waters, although Kuroshio waters of oligotrophic nature may also play a role in shaping the nutrient condition on the NSCS shelf and slope immediately off the Luzon Strait. As shown in Fig. 8, all $\delta^{30}Si_{Si(OH)_4}$ signatures collected in the upper 100 m of the water column along transect A (excluding station A9 due to the influence of significant river inputs) are close to values predicted by the steady state model assuming an initially $Si(OH)_4$-rich deep waters, whereas over half of the $\delta^{30}Si_{BSi}$ data points fall below the theoretical evolution curve. This large $\delta^{30}Si_{BSi}$ deviation partly originates from the fact that the steady state model implies the absence of BSi accumulation and thus oversimplifies the natural settings (Fripiat et al., 2011b). In other words, $\delta^{30}Si_{Si(OH)_4}$ is more rigorously applicable in model calculations since BSi has a finite but variable residence time in the upper ocean (Varela et al., 2004). As a consequence, biological fractionation by diatoms significantly controlled the $\delta^{30}Si$ dynamics in the upper 100 m of the water column on the shelf and slope in the NSCS. Moreover, the consistent decrease of $\delta^{30}Si_{Si(OH)_4}$ and $\delta^{30}Si_{BSi}$ in the upper 100 m of the water column at station A2 in summer (Fig. 3) indicates that in situ diatom growth indeed occurred throughout the entire euphotic zone.

4.5. Physical mixing controlling $\delta^{30}Si$ dynamics at station SEATS in the NSCS basin

4.5.1. Convergence of $\delta^{30}Si_{Si(OH)_4}$ and $\delta^{30}Si_{BSi}$ in surface waters: Horizontal mixing of highly fractionated waters

The highest surface $\delta^{30}Si_{Si(OH)_4}$ signature of $+2.9 \pm 0.3‰$ was observed at station SEATS in the deep basin (Fig. 4; Table 1). Within analytical error, this value is identical to the $\delta^{30}Si_{Si(OH)_4}$ of ~+2.5‰ calculated following the steady state model assuming the same initial condition and $^{30}\varepsilon_{upt}$ as for station A5 in winter. This apparent agreement suggests that the primary source of nutrients to the surface water at station SEATS may also have been the waters underlying the euphotic zone. However, $\delta^{30}Si_{BSi}$ can never exceed the initial $\delta^{30}Si_{Si(OH)_4}$ value during the isotopic evolution in an open system (Eq. (6)). Our observed $\delta^{30}Si_{BSi}$ in the surface water (also in waters at 25 m) at station SEATS in both summer and winter were equal to the corresponding $\delta^{30}Si_{Si(OH)_4}$ and significantly higher than the assumed initial $\delta^{30}Si_{Si(OH)_4}$ value of $+1.5 \pm 0.2‰$ by vertical mixing. A possible interference to the $\delta^{30}Si_{BSi}$ signatures at station SEATS is the involvement of radiolarians in the particulate samples, since the Si content of radiolarians (at the level of nmol Si per individual; Takahashi and Honjo, 1981) can be three orders of magnitude higher than that of diatoms (at the level of pmol Si per cell; Brzezinski, 1985) in seawater with very low BSi concentrations. However, the overall high $\delta^{30}Si_{BSi}$ observed at station SEATS (Fig. 5a and b) suggests negligible contribution of radiolarians to the BSi composition as their $\delta^{30}Si$ signatures (Wu et al., 1997) are on average lighter than those of diatoms.

Dissolution of BSi may lead to higher $\delta^{30}Si_{BSi}$ in the diatoms valves and correspondingly lower $\delta^{30}Si_{Si(OH)_4}$ in the surrounding water (Demarest et al., 2009) and will thus result in a decrease of $\Delta^{30}Si$ (Eq. (7)). De La Rocha et al. (2011) have proposed that isotope fractionation during BSi dissolution is the most likely cause for the notably low $\delta^{30}Si_{Si(OH)_4}$ in $Si(OH)_4$-depleted surface waters off the Kerguelen Plateau in the Southern Ocean. BSi dissolution can be enhanced by bacterial degradation of the organic layer around the valves (Bidle and Azam, 1999; Bidle et al., 2002), which probably also occurs in the surface water at station SEATS as supported by the generally low particulate organic carbon export relative to the PP in the SCS basin (Cai et al., 2008, 2010).

At the same time, however, assuming a fractionation with $^{30}\varepsilon_{diss} = -0.55‰$ given by Demarest et al. (2009), the observed $\Delta^{30}Si$ of ~0‰ in the surface water at station SEATS (Table 1) would require a BSi dissolution rate of nearly double of its production rate, which is unlikely under steady state conditions (see Demarest et al., 2009, Fig. 3). Direct reports on the BSi dissolution rate of the SCS basin are scarce. However, ~46% and ~80% of the BSi produced in the euphotic zone are found to be dissolved in the upper 150 m of the water column at station ALOHA (A Long-

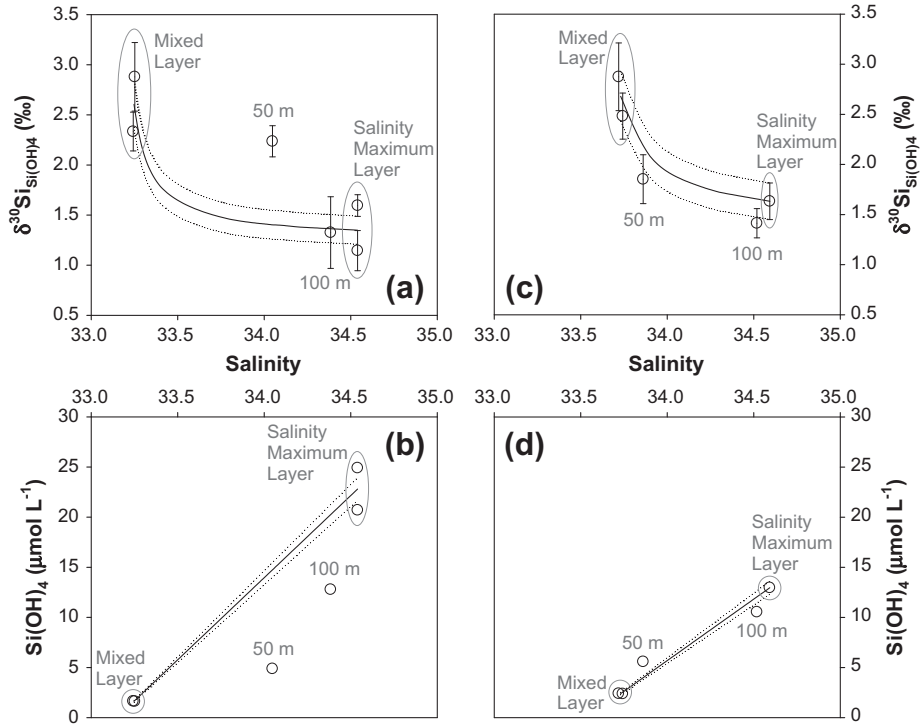

Fig. 9. $\delta^{30}Si_{Si(OH)_4}$ and $Si(OH)_4$ versus salinity for waters above the salinity maximum layer (~150–200 m) at station SEATS. The solid line in each panel represents the mixing curve between the surface mixed layer waters (above 50 m) and waters near the salinity maximum layer. Dotted lines above and below indicate errors deduced from the uncertainties in estimating the end-member values. (a) Summer: $\delta^{30}Si_{Si(OH)_4}$ versus salinity; (b) Summer: $Si(OH)_4$ versus salinity; (c) Winter: $\delta^{30}Si_{Si(OH)_4}$ versus salinity; and (d) Winter: $Si(OH)_4$ versus salinity.

term Oligotrophic Habitat Assessment) in the North Pacific (Brzezinski et al., 2011) and at station BATS (Bermuda Atlantic Time-series Study) in the North Atlantic (Nelson and Brzezinski, 1997), respectively. As also located in an oligotrophic environment, the fraction of BSi dissolution relative to its production at station SEATS is possibly lower than or between these two values for surface waters, which in any case could not result in $\delta^{30}Si_{BSi}$ being equal to $\delta^{30}Si_{Si(OH)_4}$. On the other hand, we note that the $^{30}\varepsilon_{diss}$ of −0.55‰ has been so far the only reported value on the basis of few laboratory culture experiments, which might not be valid for all natural systems. We therefore contend that additional field studies investigating the $^{30}\varepsilon_{diss}$ in natural settings combined with direct measurements of BSi production and dissolution rates are warranted to further examine the impact of BSi dissolution on $\delta^{30}Si$ signatures. In this context, while we cannot completely rule out isotopic effects of BSi dissolution, fractionation during diatom growth on the basis of $Si(OH)_4$ supplied by vertical mixing is insufficient to fully describe the dissolved and particulate $\delta^{30}Si$ distribution in the surface water at station SEATS.

Alternatively, the observed pattern of $\delta^{30}Si_{BSi}$ being equal to $\delta^{30}Si_{Si(OH)_4}$ might be interpreted as complete $Si(OH)_4$ utilization by diatoms, by which the isotopic signature of the dissolved $Si(OH)_4$ was completely transformed to the BSi product. And the pool with high $\delta^{30}Si_{Si(OH)_4}$ (+2.5‰ on average for the top 25 m waters) might have originated from horizontal admixture of highly fractionated waters, such as surface waters from the nearby slope area. Another possible process that could contribute to such a fractionated Si isotopic signature is mesoscale eddies propagated from elsewhere. Complete $Si(OH)_4$ consumption by diatoms to undetectable levels has for example been observed at the base of the euphotic zone within a mode water mesoscale eddy off Bermuda (McNeil et al., 1999). Eddies frequently occur in the SCS (e.g., Wu and Chiang, 2007; Nan et al., 2011). For instance, an anticyclonic eddy observed in August 2007 at the position around station SEATS has a life history of near six months since its formation (Nan et al., 2011). Such long-lived eddies may likely have experienced $Si(OH)_4$ overconsumption leading to high degrees of Si isotope fractionations. However, how significantly eddies can influence the hydrography and chemistry at station SEATS needs further examination. Nevertheless, the observed patterns clearly indicate that the $\delta^{30}Si_{BSi}$ and the $\delta^{30}Si_{Si(OH)_4}$ signatures in surface waters at station SEATS were formed at different times and not from the same source waters.

4.5.2. Vertical $\delta^{30}Si_{Si(OH)_4}$ gradients in the upper 100 m largely induced by diapycnal mixing

During the sampling period, the mixed layer depth at station SEATS in summer was ~30 m while in winter it was deeper but still less than 50 m. As a consequence, it does not seem possible that nutrients from deeper waters have been upwelled or mixed into the surface mixed layer,

which is generally shallower than the nutricline in the deep basin of the NSCS (Tseng et al., 2005). Rather than being induced by the upward increasing biological utilization of $Si(OH)_4$ delivered into the euphotic zone from underlying waters, the downward decreasing trend of $\delta^{30}Si_{Si(OH)_4}$ in the upper 100 m of the water column at station SEATS might simply result from diapycnal mixing via for instance vertical diffusion (Tian et al., 2009) between high $\delta^{30}Si_{Si(OH)_4}$ surface waters and waters below the euphotic zone with low $\delta^{30}Si_{Si(OH)_4}$.

To examine this potential mechanism, we constructed the mixing curve for both $\delta^{30}Si_{Si(OH)_4}$ and $Si(OH)_4$ between the surface mixed layer waters and waters around the salinity maximum layer (Fig. 9). Within analytical error, only the data point of $\delta^{30}Si_{Si(OH)_4}$ at 50 m in summer is above the mixing curve while all other data points in the euphotic zone fall on the mixing curve (Fig. 9a and c). Correspondingly, the largest $Si(OH)_4$ deficit of $\sim$10 μmol L^{-1} relative to the value predicted from mixing was also observed at 50 m in summer (Fig. 9b) suggesting that diatom growth at this depth consumed a large amount of dissolved $Si(OH)_4$ and resulted in high $\delta^{30}Si_{Si(OH)_4}$. Taking the $\delta^{30}Si_{Si(OH)_4}$ of $+1.4 \pm 0.2‰$ and $Si(OH)_4$ of $\sim$15 μmol L^{-1} predicted from mixing as initial condition (Fig. 9a and b), $^{30}\varepsilon_{upt}$ at 50 m at station SEATS in summer was estimated to be $-0.7 \pm 0.2‰$ by the Rayleigh model (Eq. (1)) and $-1.2 \pm 0.4‰$ by the steady state model (Eq. (5)). Both values are in agreement with the consensus fractionation factor of $-1.1 \pm 0.4‰$ (De La Rocha et al., 1997) as well as the directly observed $\Delta^{30}Si$ of $-0.9 \pm 0.2‰$ (Table 1). As a consequence, the two end-member mixing scheme combined with limited biological fractionation can describe the vertical $\delta^{30}Si_{Si(OH)_4}$ gradients in the euphotic zone at station SEATS.

4.5.3. Heavier $\delta^{30}Si_{BSi}$ than $\delta^{30}Si_{Si(OH)_4}$ below the surface mixed layer: Sinking of high-$\delta^{30}Si_{BSi}$ particles and upwelling of low-$\delta^{30}Si_{Si(OH)_4}$ waters

In contrast to the biologically mediated low $\delta^{30}Si_{BSi}$ at 50 m in summer, $\delta^{30}Si_{BSi}$ at 50 m in winter was heavier than the corresponding $\delta^{30}Si_{Si(OH)_4}$ and nearly the same as $\delta^{30}Si_{BSi}$ values in the top 25 m waters (Fig. 5b). Noteworthy is that BSi concentrations displayed a maximum at 50 m depth in the euphotic zone in summer whereas a minimum was observed in winter (Fig. 5c), even though the chlorophyll maximum layer was located around 50 m in both seasons at station SEATS (data not shown). We contend that BSi in the latter case was composed mainly of diatoms that settled out from the waters above rather than being produced in situ. This viewpoint is consistent with the hypothesis that physical mixing without biological fractionation may have caused the $\delta^{30}Si_{Si(OH)_4}$ value at 50 m in winter, as well as at 100 m during both seasons (Fig. 9c). $\delta^{30}Si_{BSi}$ at 100 m water depth at station SEATS displayed no seasonal variations and both values were also higher than the corresponding $\delta^{30}Si_{Si(OH)_4}$ (Fig. 5a and b).

$\delta^{30}Si_{BSi}$ in deep waters at station SEATS (also at stations A2 and A10, Fig. 3) were comparable to at least one value in the upper 100 m of the water column (Fig. 5a and b), as BSi at depth must completely originate from the euphotic zone. $\delta^{30}Si_{BSi}$ values below 100 m in summer at station SEATS were lower than those in the surface mixed layer but higher than that at a depth of 50 m (Fig. 5a). Diatoms collected below the euphotic zone might thus represent a mixture of settled diatoms from both the mixed layer and waters at 50 m. In fact, the weighted mean $\delta^{30}Si_{BSi}$ values were calculated at $+1.9 \pm 0.1‰$ and $+2.0 \pm 0.1‰$, respectively, for the upper 50 m and waters between 100 m and 500 m, which is a very good agreement. In winter, $\delta^{30}Si_{BSi}$ values below 100 m at station SEATS were overall comparable to those in the mixed layer (Fig. 5b). Such preservation of $\delta^{30}Si_{BSi}$ signatures during both seasons suggests negligible isotopic effects of BSi dissolution in waters below 100 m at station SEATS. As a consequence, diatom growth at station SEATS should primarily occur in the mixed layer above 50 m depth and contribute to the majority of BSi below. This way, the high $\delta^{30}Si_{BSi}$ signatures in surface waters were transmitted to underlying waters where the $\delta^{30}Si_{Si(OH)_4}$ were, however, diluted by rapid upward mixing of low $\delta^{30}Si_{Si(OH)_4}$ waters, which ultimately were lower than $\delta^{30}Si_{BSi}$. Through examining C isotopic compositions, Liu et al. (2007) have also demonstrated that suspended particulate organic carbon from the top 50 m waters at station SEATS is the major source for sinking particles at depth.

4.6. Surface $\delta^{30}Si_{Si(OH)_4}$ gradients in the NSCS

Surface $\delta^{30}Si_{Si(OH)_4}$ generally increased from $\sim+2.3‰$ on the inner shelf to $\sim+2.5‰$ above the outer shelf and slope and finally to $\sim+2.8‰$ above the deep basin, suggesting increasing fractionation during the transition from eutrophic to oligotrophic conditions in the NSCS. On the inner shelf, which is fed by the Pearl River inputs, the signature of biological fractionation was weaker due to the relatively low degree of $Si(OH)_4$ utilization caused by continuous supply of Si. In the deep basin however, the heavier surface $\delta^{30}Si_{Si(OH)_4}$ resulted from the more complete consumption of the available $Si(OH)_4$.

5. CONCLUSIONS

The dynamics of $\delta^{30}Si$ in the NSCS were overall controlled by the combination of physical mixing, biological utilization and to some extent BSi dissolution. Spatial variations influenced by asynchronous formation of the $\delta^{30}Si_{BSi}$ and the $\delta^{30}Si_{Si(OH)_4}$ signatures were distinctly more important than seasonal variations.

Surface $\delta^{30}Si_{Si(OH)_4}$ displayed a slight but significant increase from the inner shelf to the deep basin as a function of increasing $Si(OH)_4$ utilization along the transition from eutrophic to oligotrophic conditions. In the euphotic zone at various stations located on the NSCS shelf and slope, $\delta^{30}Si_{BSi}$ signatures were found systematically lower than the corresponding $\delta^{30}Si_{Si(OH)_4}$. This expected pattern combined with overall high BSi production suggests biological fractionation of Si isotopes from $Si(OH)_4$-rich initial source waters. The processes mainly responsible for this situation were the Pearl River input for surface waters on the inner

shelf, and upwelling or vertical mixing for waters in the euphotic zone on the outer shelf and slope.

On the other hand, while the wind-induced mixing was unable to deliver $Si(OH)_4$ from depth into the shallow surface mixed layer for further biological utilization at station SEATS located in the oligotrophic NSCS basin, diapycnal mixing between high $\delta^{30}Si_{Si(OH)_4}$ surface waters and low $\delta^{30}Si_{Si(OH)_4}$ deep waters dominated the vertical distribution of $\delta^{30}Si_{Si(OH)_4}$ through the entire water column and active Si isotope fractionation by diatoms at this location was less important. An atypical pattern of $\delta^{30}Si_{BSi}$ being equal to or even higher than $\delta^{30}Si_{Si(OH)_4}$ was observed in the euphotic zone at station SEATS, which cannot be explained by either Rayleigh or steady state models with an initial condition of $Si(OH)_4$-rich deep waters. We envision that rapid horizontal mixing with highly fractionated waters primarily contributed to the nutrients available in the surface mixed layer at station SEATS, in which the following nearly complete $Si(OH)_4$ utilization by diatoms had most likely led to relatively heavy $\delta^{30}Si_{BSi}$. Moreover, BSi collected from subsurface waters below was mainly supplied by sinking from the surface mixed layer and thus inherited the heavy $\delta^{30}Si_{BSi}$ characteristic.

In this study, the Rayleigh and steady state models were used to validate the assumed initial conditions rather than to estimate the $^{30}\varepsilon_{upt}$. While the consensus value of $^{30}\varepsilon_{upt} = -1.1 \pm 0.4‰$ (De La Rocha et al., 1997) is overall also consistent with the observed Si isotope fractionation by diatoms in different areas of the NSCS, the initial conditions have largely been controlled by variable mixing between differently fractionated Si pools. In this context, it is important to distinguish biological fractionation of Si isotopes from the effects of water mass mixing in highly dynamic marginal systems such as the NSCS.

ACKNOWLEDGEMENTS

This study was conducted in the framework of the CHOICE-C project (Carbon cycling in China Seas – budget, controls and ocean acidification) which was financially supported by the National Basic Research Program of China (973 Program) through grant 2009CB421201. This study was also supported by the National Science Foundation of China through grant 41121091. We would like to thank Danna Wang, Tao Huang, Chuanjun Du, and Hua Lin for help with the ancillary data collection and the crew of R/V *Dongfanghong II* for their assistance in sample collection. We thank Jianyu Hu for providing the CTD data and Jun Sun for providing the chlorophyll data. We are also grateful to the inspiring comments from Kon-Kee Liu, Zhiyu Liu and Shuh-Ji Kao. Comments from three anonymous reviewers have significantly improved the quality of the paper.

REFERENCES

Abraham K., Opfergelt S., Fripiat F., Cavagna A.-J., de Jong J. T. M., Foley S. F., André L. and Cardinal D. (2008) Δ^{30}Si and δ^{29}Si determinations on USGS BHVO-1 and BHVO-2 reference materials with a new configuration on an Nu Plasma Multi-Collector ICP-MS. *Geostand. Geoanal. Res.* **32**, 193–202.

Albarède F., Telouk P., Blichert-Toft J., Boyet M., Agranier A. and Nelson B. (2004) Precise and accurate isotopic measurements using multiple-collector ICPMS. *Geochim. Cosmochim. Acta* **68**, 2725–2744.

Beucher C. P., Brzezinski M. A. and Jones J. L. (2008) Sources and biological fractionation of Silicon isotopes in the Eastern Equatorial Pacific. *Geochim. Cosmochim. Acta* **72**, 3063–3073.

Beucher C. P., Brzezinski M. A. and Jones J. L. (2011) Mechanisms controlling silicon isotope distribution in the Eastern Equatorial Pacific. *Geochim. Cosmochim. Acta* **75**, 4286–4294.

Bidle K. D. and Azam F. (1999) Accelerated dissolution of diatom silica by marine bacterial assemblages. *Nature* **397**, 508–512.

Bidle K. D., Manganelli M. and Azam F. (2002) Regulation of oceanic silicon and carbon preservation by temperature control on bacteria. *Science* **298**, 1980–1984.

Brzezinski M. A. (1985) The Si:C:N ratio of marine diatoms: Interspecific variability and the effect of some environmental variables. *J. Phycol.* **21**, 347–357.

Brzezinski M. A. and Phillips D. R. (1997) Evaluation of ^{32}Si as a tracer for measuring silica production rates in marine waters. *Limnol. Oceanogr.* **42**, 856–865.

Brzezinski M. A., Jones J. L., Beucher C. P., Demarest M. S. and Berg H. L. (2006) Automated determination of silicon isotope natural abundance by the acid decomposition of cesium hexafluosilicate. *Anal. Chem.* **78**, 6109–6114.

Brzezinski M. A., Krause J. W., Church M. J., Karl D. M., Li B., Jones J. L. and Updyke B. (2011) The annual silica cycle of the North Pacific subtropical gyre. *Deep Sea Res. Part I* **58**, 988–1001.

Cai P., Chen W., Dai M., Wan Z., Wang D., Li Q., Tang T. and Lv D. (2008) A high-resolution study of particle export in the southern South China Sea based on ^{234}Th:^{238}U disequilibrium. *J. Geophys. Res.* **113**, C04019. http://dx.doi.org/10.1029/2007JC004268.

Cai P., Rutgers van der Loeff M., Stimac I., Nöthig E.-M., Lepore K. and Moran S. B. (2010) Low export flux of particulate organic carbon in the central Arctic Ocean as revealed by 234Th:238U disequilibrium. *J. Geophys. Res.* **115**, C10037. http://dx.doi.org/10.1029/2009JC005595.

Cai W.-J., Dai M., Wang Y., Zhai W., Huang T., Chen S., Zhang F., Chen Z. and Wang Z. (2004) The biogeochemistry of inorganic carbon and nutrients in the Pearl River estuary and the adjacent Northern South China Sea. *Cont. Shelf Res.* **24**, 1301–1319.

Cao Z. and Dai M. (2011) Shallow-depth $CaCO_3$ dissolution: Evidence from excess calcium in the South China Sea and its export to the Pacific Ocean. *Global Biogeochem. Cycles* **25**, GB2019. http://dx.doi.org/10.1029/2009GB003690.

Cao Z., Dai M., Zheng N., Wang D., Li Q., Zhai W., Meng F. and Gan J. (2011) Dynamics of the carbonate system in a large continental shelf system under the influence of both a river plume and coastal upwelling. *J. Geophys. Res.* **116**, G02010. http://dx.doi.org/10.1029/2010JG001596.

Cardinal D., Alleman L. Y., Dehairs F., Savoye N., Trull T. W. and Andre L. (2005) Relevance of silicon isotopes to Si-nutrient utilization and Si-source assessment in Antarctic waters. *Global Biogeochem. Cycles* **19**. http://dx.doi.org/10.1029/2004GB002364.

Cardinal D., Savoye N., Trull T. W., Dehairs F., Kopczynska E. E., Fripiat F., Tison J.-L. and André L. (2007) Silicon isotopes in spring Southern Ocean diatoms: Large zonal changes despite homogeneity among size fractions. *Mar. Chem.* **106**, 46–62.

Cavagna A.-J., Fripiat F., Dehairs F., Wolf-Gladrow D., Cisewski B., Savoye N., André L. and Cardinal D. (2011) Silicon uptake and supply during a Southern Ocean iron fertilization experiment (EIFEX) traced by Si isotope. *Limnol. Oceanogr.* **56**, 147–160.

Chao S. Y., Shaw P. T. and Wu S. Y. (1996) Deep water ventilation in the South China Sea. *Deep Sea Res. Part II* **43**, 445–466.

Chen Y. L. L. (2005) Spatial and seasonal variations of nitrate-based new production and primary production in the South China Sea. *Deep Sea Res. Part I* **52**, 319–340.

Chen J., Huang B., Liu Y., Cao Z. and Hong H. (2006) Phytoplankton community structure in the transects across East China Sea and northern South China Sea determined by analysis of HPLC photosynthetic pigment signatures. *Adv. Earth Sci.* **21**, 738–746 (in Chinese).

Chern C.-S., Wang J. and Wang D.-P. (1990) The exchange of Kuroshio and East China Sea shelf water. *J. Geophys. Res.* **95**, C9. http://dx.doi.org/10.1029/JC095iC09p16017.

Dai M., Zhai W., Cai W.-J., Callahan J., Huang B., Shang S., Huang T., Li X., Lu Z., Chen W. and Chen Z. (2008) Effects of an estuarine plume-associated bloom on the carbonate system in the lower reaches of the Pearl River estuary and the coastal zone of the northern South China Sea. *Cont. Shelf Res.* **28**, 1416–1423.

Dai M., Meng F., Tang T., Kao S.-J., Lin J., Chen J., Huang J.-C., Tian J., Gan J. and Yang S. (2009) Excess total organic carbon in the intermediate water of the South China Sea and its export to the North Pacific. *Geochem. Geophys. Geosyst.* **10**, Q12002. http://dx.doi.org/10.1029/2009GC002752.

De La Rocha C. L., Brzezinski M. A. and DeNiro M. J. (1997) Fractionation of silicon isotopes during biogenic silica formation. *Geochim. Cosmochim. Acta* **61**, 5051–5056.

De La Rocha C. L., Brzezinski M. A. and DeNiro M. J. (2000) A first look at the distribution of the stable isotopes of silicon in natural water. *Geochim. Cosmochim. Acta* **64**, 2467–2477.

De La Rocha C. L., Bescont P., Croguennoc A. and Ponzevera E. (2011) The silicon isotopic composition of surface waters in the Atlantic and Indian sectors of the Southern Ocean. *Geochim. Cosmochim. Acta* **75**, 5283–5295.

Demarest M. S., Brzezinski M. A. and Beucher C. P. (2009) Fractionation of silicon isotopes during biogenic silica dissolution. *Geochim. Cosmochim. Acta* **73**, 5572–5583.

de Souza G. F., Reynolds B. C., Rickli J., Frank M., Saito M. A., Gerringa L. J. A. and Bourdon B. (2012) Southern Ocean control of silicon stable isotope distribution in the deep Atlantic Ocean. *Global Biogeochem. Cycles* **26**, GB2035. http://dx.doi.org/10.1029/2011GB004141.

Douthitt C. B. (1982) The geochemistry of the stable isotopes of silicon. *Geochim. Cosmochim. Acta* **46**, 1449–1458.

Fripiat F., Corvaisier R., Navez J., Elskens M., Schoemann V., Leblanc K., André L. and Cardinal D. (2009) Measuring production-dissolution rates of marine biogenic silica by ^{30}Si-isotope dilution using a high-resolution sector field inductively coupled plasma mass spectrometer. *Limnol. Oceanogr. Methods* **7**, 470–478.

Fripiat F., Cavagna A.-J., Dehairs F., Speich S., André L. and Cardinal D. (2011a) Silicon pool dynamics and biogenic silica export in the Southern Ocean inferred from Si-isotopes. *Ocean Sci.* **7**, 533–547.

Fripiat F., Cavagna A.-J., Savoye N., Dehairs F., André L. and Cardinal D. (2011b) Isotopic constraints on the Si-biogeochemical cycle of the Antarctic Zone in the Kerguelen area (KEOPS). *Mar. Chem.* **123**, 11–22.

Fripiat F., Cavagna A.-J., Dehairs F., de Brauwere A., André L. and Cardinal D. (2012) Processes controlling the Si-isotopic composition in the Southern Ocean and application for paleoceanography. *Biogeosciences* **9**, 2443–2457.

Georg R. B., Reynolds B. C., Frank M. and Halliday A. N. (2006a) Mechanisms controlling the silicon isotopic compositions of river waters. *Earth Planet. Sci. Lett.* **249**, 290–306.

Georg R. B., Reynolds B. C., Frank M. and Halliday A. N. (2006b) New sample preparation techniques for the determination of Si isotopic compositions using MC-ICPMS. *Chem. Geol.* **235**, 95–104.

Gong G. C., Liu K.-K., Liu C. T. and Pai S. C. (1992) The chemical hydrography of the South China Sea west of Luzon and a comparison with the West Philippine Sea. *Terr. Atmos. Ocean. Sci.* **3**, 587–602.

Guo X. H., Cai W.-J., Zhai W. D., Dai M. H., Wang Y. C. and Chen B. S. (2008) Seasonal variations in the inorganic carbon system in the Pearl River (Zhujiang) estuary. *Cont. Shelf Res.* **28**, 1424–1434.

Han A., Dai M., Kao S.-J., Gan J., Li Q., Wang L., Zhai W. and Wang L. (2012) Nutrient dynamics and biological consumption in a large continental shelf system under the influence of both a river plume and coastal upwelling. *Limnol. Oceanogr.* **57**, 486–502.

Hendry K. R., Georg R. B., Rickaby R. E. M., Robinson L. F. and Halliday A. N. (2010) Deep ocean nutrients during the Last Glacial Maximum deduced from sponge silicon isotopic compositions. *Earth Planet. Sci. Lett.* **292**, 290–300.

Karl D. M. and Tien G. (1992) MAGIC: A sensitive and precise method for measuring dissolved phosphorus in aquatic environments. *Limnol. Oceanogr.* **37**, 105–116.

Liu K.-K., Kao S.-J., Hu H.-C., Chou W.-C., Hung G.-W. and Tseng C.-M. (2007) Carbon isotopic composition of suspended and sinking particulate organic matter in the northern South China Sea-From production to deposition. *Deep Sea Res. Part II* **54**, 1504–1527.

Liu Z., Xu J., Li L. and Shi M. (2001) Characteristics and distribution of water masses in the South China Sea during summer and winter of 1998. In *Oceanography in China* (eds. H. Xue, F. Chai and J. Xu). China Ocean Press, Beijing, pp. 221–230 (in Chinese).

McNeil J. D., Jannasch H. W., Dickey T., McGillicuddy D., Brzezinski M. and Sakamoto C. M. (1999) New chemical, bio-optical and physical observations of upper ocean response to the passage of a mesoscale eddy off Bermuda. *J. Geophys. Res.* **104**, 15537–15548. http://dx.doi.org/10.1029/1999JC900137.

Nan F., He Z., Zhou H. and Wang D. (2011) Three long-lived anticyclonic eddies in the northern South China Sea. *J. Geophys. Res.* **116**, C05002. http://dx.doi.org/10.1029/2010JC006790.

Nelson D. M. and Brzezinski M. A. (1997) Diatom growth and productivity in an oligotrophic midocean gyre: A 3-yr record from the Sargasso Sea near Bermuda. *Limnol. Oceanogr.* **42**, 473–486.

Nelson D. M., Tréguer P., Brzezinski M. A., Leynaert A. and Quéguiner B. (1995) Production and dissolution of biogenic silica in the ocean: Revised global estimates, comparison with regional data and relationship to biogenic sedimentation. *Global Biogeochem. Cycles* **9**, 359–372.

Ning X., Chai F., Xue H., Cai Y., Liu C. and Shi J. (2004) Physical–biological oceanographic coupling influencing phytoplankton and primary production in the South China Sea. *J. Geophys. Res.* **109**, C10005. http://dx.doi.org/10.1029/2004JC002365.

Qu T. (2000) Upper-layer circulation in the South China Sea. *J. Phys. Oceanogr.* **30**, 1450–1460.

Qu T., Mitsudera H. and Yamagata T. (2000) Intrusion of the North Pacific waters into the South China Sea. *J. Geophys. Res.* **105**, C3. http://dx.doi.org/10.1029/1999JC900323.

Ragueneau O., Savoye N., Del Amo Y., Cotten J., Tardiveau B. and Leynaert A. (2005) A new method for the measurement of biogenic silica in suspended matter of coastal waters: Using

Si:Al ratios to correct for the mineral interference. *Cont. Shelf Res.* **25**, 697–710.

Reynolds B. C., Frank M. and Halliday A. N. (2006) Silicon isotope fractionation during nutrient utilization in the North Pacific. *Earth Planet. Sci. Lett.* **244**. http://dx.doi.org/10.1016/j.epsl.2006.02.002.

Reynolds B. C., Aggarwal J. and André L., et al. (2007) An inter-laboratory comparison of Si isotope reference materials. *J. Anal. At. Spectrom.* **22**, 561–568.

Takahashi K. and Honjo S. (1981) Vertical flux of Radiolaria: A taxon-quantitative sediment trap study from the western tropical Atlantic. *Micropaleontology* **27**, 140–190.

Tian J., Yang Q. and Zhao W. (2009) Enhanced diapycnal mixing in the South China Sea. *J. Phys. Oceanogr.* **39**, 3191–3203.

Tseng C.-M., Wong G. T. F., Lin I.-I., Wu C.-R. and Liu K.-K. (2005) A unique seasonal pattern in phytoplankton biomass in low-latitude waters in the South China Sea. *Geophys. Res. Lett.* **32**, L08608. http://dx.doi.org/10.1029/2004GL022111.

Varela D. E., Pride C. J. and Brzezinski M. A. (2004) Biological fractionation of silicon isotopes in Southern Ocean surface waters. *Global Biogeochem. Cycles* **18**, GB1047. http://dx.doi.org/10.1029/2003GB002140.

Wang J.-B., Li X.-Z. and Tan Z.-Y. (2005) Species composition and distribution of polycystine radiolarians (Protozoa) in the planton from the northwestern South China Sea. *Acta Oceanol. Sin.* **27**, 100–106 (in Chinese).

Wong G. T. F., Ku T.-L., Mulholland M., Tseng C.-M. and Wang D.-P. (2007) The South East Asian Time-series Study (SEATS) and the biogeochemistry of the South China Sea-An overview. *Deep Sea Res. Part II* **54**, 1434–1447.

Wu C.-R. and Chiang T.-L. (2007) Mesoscale eddies in the northern South China Sea. *Deep Sea Res. Part II* **54**, 1575–1588.

Wu S., Ding T., Meng X. and Bai L. (1997) Determination and geological implication of O–Si isotope of the sediment core in the CC area, the Pacific Ocean. *Chin. Sci. Bull.* **42**, 1462–1465.

Young E. D., Galy A. and Nagahara H. (2002) Kinetic and equilibrium mass-dependent isotope fractionation laws in nature and their geochemical and cosmochemical significance. *Geochim. Cosmochim. Acta* **66**, 1095–1104.

Associate Editor: James McManus